People's Democratic Republic of Algeria

Ministry of Higher Education and Scientific Research

University Center of Ahmed Ben YahiaEl-Wancharissi–Tissemsilt

Institute of Sciences and Technology

Department of Sciences and Technology

Dissertation submitted in fulfillment of the requirements for the degree of academic Master in

Stream: **Mechanical Engineering**

Specialty: **Energy Installation and Turbomachinery**

Realized by: **BEGHAMI Mohamed Abdelillah**

Theme

Study of mesh sensitivity in CFD and the influence of turbulence models on numerical calculations

---

November 2020

Board of Examiners:

Dr. KAHIL Y.	Supervisor	Tissemsilt U. C.
Dr. BENLEKKAM M.	Examiner	Tissemsilt U. C.
Dr. MERGHACHE M.	Examiner	Tissemsilt U. C.

2019-2020

Acknowledgments

All the gratitude and thanks to God our creator who has given us the strength to carry out and complete this work.

First of all, I would like to thank the members of the jury, the president **Dr. BENLEKAM M**. and **Dr.MERGHACHE**to agree to examine this modest memory.

I would like to thank my promoter very warmly **Dr. KAHIL Y.** for having proposed this subject to me, for its precious advice for his open-mindedness and availability.

Many thanks to all the professors of the department of Science and Technology for their contribution to my education and training, and my knowledge.

Dedication

“Everything I am or ever will be, I owe it to my mother

My success is because of her, and my failures are because of me.

To you mother.

“To my biggest supporter

To you father “

To all my family

to all my friends and colleagues.

Table of contents

List of figures

List of tables

Nomenclature

M	Mass
ρ	fluid density$[kg/m^3]$
U	mean fluid velocity$[m.s^{-1}]$
P	Pressure
$\vec{A}$	surface area vector
C_μ	constants of the K-ε model
μ	dynamic viscosity of the fluid $[P_a s^{-1}]$
L	integral scale
u′	fluctuating component
N	grid number
Re	Reynolds number
$\overline{u}$	time-averaged velocity
s_{ij}	train-rate tensor
v_T	turbulent eddy viscosity
k	turbulence kinetic energy
v	molecular viscosity
$\overline{v}$	transport equations
C_{w1}	ω production
S	invariant measure of the deformation rate
Ω_{ij}	rotation tensor
$C_{\varepsilon 1}, C_{\varepsilon 2}, \delta_k, \delta_\varepsilon$	coefficients of k-ε modeling
$\overline{u_\iota' u_j'}$	components of Reynolds tensor.
$\alpha, \beta_0^*, \delta^* \beta_0$	coefficients of k-ω modeling
P_k	production limiter
F_1	blending function
F_2	second blending function
$\beta^*, \alpha_1, \beta_1, \delta_{k1}, \delta_{\omega 1}, \alpha_2, \delta_{k2}, \delta_{\omega 2}$	coefficients of k-ω-SST model
$\vec{v}$	velocity vector $\left(\vec{v} = v_x \vec{\imath} + v_y \vec{\jmath}\right)$
Γ_ϕ	diffusion coefficient of the quantityϕ.
$\overrightarrow{grad}\phi$	gradient of ϕ
S_ϕ	source term (the source of Φ per unit of volume).
ϕ_f	convection transfer value cross the interface Φ
v_f	mass flow through the interface f

$\frac{1}{2}\rho U^2$	kinetic energy
$\overline{Ux}/U_0$	mean streamwise velocity
$\overline{C_P}$	mean pressure coefficient
$\bar{P}$	average pressure
P_∞	initial pressure
u_0	initial velocity
N_{faces}	number of faces of the control volume

Acronyms

ALE	Arbitrary Lagrangian-Eulerian
MRL	Momentum Reversal Lift
IBF	Immersed Body Force
CHT	Convective Heat Transfer
PLT	Prismatic Layer Thicknesses
ATR	Agitated Tubular Reactor
FSI	Fluid Structure Interactions
VOF	Volume Of Fluid
RMSE	Root Mean Square Error
RMDHL	Reciprocating Mechanism Driven Heat Loops
SCWRs	Super Critical pressure Water-cooled Reactors
LES	Large Eddy Simulation
RSM	Reynolds Stress Model
DNS	Direct Numerical Simulation
SGS	Sub Grid Scale
FVM	Finite Volume Method

GENERAL INTRODUCTION

General introduction

Computational Fluid Dynamics (CFD) is the simulation of fluids engineering systems using modeling (mathematical physical problem formulation) and numerical methods (discretization methods, solvers, numerical parameters, and grid generations, etc.) **[1].** The first idea of CFD calculation appeared in England (1881-1953) (in a modern sense) although Lewis Fry Richardson developed the first numerical weather prediction system when he divided physical space into grid cells and used the finite difference approximations of Bjerknes's "primitive differential equations", During the 1960s,in the USA the theoretical division of (NASA) contributed many numerical methods that are still in use in CFD today, such as the ubiquitous $k-\varepsilon$ turbulence model, and the arbitrary lagrangian-eulerian (ALE) method. In the 1970s,a group working under D. Brain in London, developed the first parabolic flow codes, (GENMIX), vorticity-stream function based codes the simple algorithm and the teach code, as well as the form of the $k-\varepsilon$ equation that are used today. In early 1980s, commercial CFD codes come into the open market **[2].**

Even simple flows are difficult to compute. The computational complexity grows exponentially when accounting for turbulence.

Turbulent flows are commonplace in most real life scenarios, including the flow of blood through the cardiovascular system **[3],** the airflow over an aircraft wing, its fluid motion characterized by chaotic changes in pressure and flow velocity. It is in contrast to a laminar flow, which occurs when a fluid flows in parallel layers, with no disruption between those layers, and to simulate turbulent flows we use turbulent models, to predict the evolution of turbulence, these turbulence models are simplified constitutive equation that predict the statistical evolution of turbulent flows, Therefore, we see that the choice of mesh is one of the most important factors to obtain good results for this reason, we will test different types of mesh and use different models of turbulence and compare them with the experimental results to choose the type of mesh.

The manuscript is divided in five chapters. We start by a bibliographic analysis; the second chapter concerns the turbulence modeling. In the third chapter we present the numerical resolution with all free software used for this work. The study cases are showed in the fourth chapter followed by the results and discussion. At the end we finish with general conclusion which regroups the essential of our study.

CHAPTER 1: BIBLIOGRAPHIC ANALYSIS

1.1 State of art

It is no secret to anyone that the CFD has acquired a major position in scientific research today, among the most important research in the CFD, which is the mesh sensitivity testing. One can find here:

Yi He et al. (2020) [4] carried out studied the flows behavior of an agitated tubular reactor using a novel dynamic mesh based CFD model.

They proposed a new CFD approach to study fluid dynamics and mixing mechanisms in the ATR (Agitated tubular reactor). They combine a soft-sphere collision model with a dynamic meshing approach on ANSYS Fluent to tackle structure-structure and fluid-structure interactions (FSI) simultaneously. The performances of Reynolds Stress Models were evaluated and pressure-strain term shows little effect on agitator's motion. The energy was found to be mainly consumed by viscous dissipation.

Hao Li et al. (2019) [5] realized a CFD prediction of convective heat transfer and pressure drop of pigs in group using virtual wind tunnels: Influence of grid resolution and turbulence

Oxygenating for the animal house is important since it is consequently linked with the convective heat removal from animals. To ponder this convective heat transfer (CHT), they used the (CFD) computational fluid dynamics, simulation accuracy is affected by grid treatment and the choice of turbulence models. To reveal the grid effects on CHT and PD, fifteen 3D meshes with different facial grids sizes (0.04 m, 0.02 m, and 0.008 m) and prismatic layer thicknesses (PLT) (0 m, 0.0015 m, 0.009 m, 0.02 m, 0.04 m) they used turbulence models, namely, standard K-ε, realisable K-ε, standard K-ω, and SST K-ω, together with two wall treatments were appraised and compared with the empirical calculation.

The results showed that the PLT could be an important influence on the stability of the simulation with varied facial grid sizes.

Zhang et al. (2019) [6] carried out a comprehensive CFD-based erosion prediction for sharp bend geometry with examination of grid effect.

These researchers did an additional confirmation of the proposed Computational Fluid Dynamics (CFD) based erosion prediction procedure for a different geometry. Special emphasis is played on the tough effects of the grids on the resulting erosion profile representation. Detailed meshing information is provided for repeatable and further improved CFD studies in future. In the process, erosion predictions for both large (256 μm) and small

particles (25 μm) in a sharp bend geometry are performed by applying the comprehensive CFD-based erosion prediction procedure.

Tsoutsaniset al. in (2015) [7] realized a comparison of structured- and unstructured-grid, compressible and incompressible methods using the vortex pairing problem.

He shed light into the numerical advantages and disadvantages of different numerical quantizing, The methods consist of structured and unstructured finite volume and Lagrange-Remap methods, with accuracy ranging from 2nd to 9th-order, with and without applying low-Mach corrections. He shows that the momentum thickness and large scale features of a basic vortical structure are well conclude even at the lowest grid resolution of 32 × 32 provided that the numerical schemes are of a high-order of accuracy or the numerical framework is sufficiently non-dissipative. The implementation of the finite volume methods in unstructured triangular meshes provides the best results even without low Mach number alteration provided that a higher-order advective discretization for the advective fluxes is employed.

Ivana Martić et al. (2017) [8] carried out a study mesh sensitivity analysis for the numerical simulation of a damaged ship model.

In their search, the numerical simulation of flow around the hole and inside the tanks and a calculation of the total resistance of the damaged model are carried out using the commercial software package STAR-CCM+. The mathematical model is based on the Reynolds Averaged Navier-Stokes (RANS) equations, with the Volume of Fluid (VOF) method for two phase turbulent flow, and the k-ε turbulence model. The mesh sensitivity analysis of the results obtained for the total resistance force of the damaged model is conducted using different mesh resolutions.

Mulualem G. et al. (2012) [9] carried out a CFD simulations for sensitivity analysis of different parameters to the wake characteristics of tidal turbine. He did an investigation in the sensitivity of mesh grid size to the wake characteristics of Momentum Reversal Lift (MRL) turbine using a new computational fluid dynamics (CFD) based Immersed Body Force (IBF) model.

The simulation results showed that the grid size and width proximity have had massive impact on the flow characteristics and the computational cost of the tidal turbine. A fine grid size and large width inflicted longer computational time.

Rui Zhang et al. (2010) [10] realized a prototype mesh generation tool for CFD simulations in architecture domain.

This paper presents an effort to apply quality mesh generation for CFD simulations in the architectural-context.
A prototype meshing tool is developed to construct adaptive quadrilateral meshes from two-dimensional image data, e.g., architecture drawings. First the quadtree based isocontouring method is utilized to generate initial uniform quadrilateral meshes in the immediate region of the objects. Meshes are further decomposed into finer quads adaptively near the surface of the object without introducing any hanging nodes. Boundary layers are then generated using the pillowing technique and the thickness of the boundary layer is controlled to achieve the desired y^+ values for different near wall turbulence models. Finally, meshes are extended to the ambient domain with desired sizes, where flow fields are assumed to be relatively steady. The developed tool has been employed to generate meshes for CFD simulations of scenarios commonly existing in the indoor and outdoor environment.

Another group of researchers were interested in studying influence of turbulence models on numerical calculations, among these researchers we find:

Jia-Wei Han et al. (2019) [11] realized a comparison of veracity and application of different CFD turbulence models for refrigerated transport.

The objective from their work was to establish a comprehensively verified 3D CFD model of this (standard κ-ω andκ-ω-SST) and to predict the temporal-spatialε (Realizable κ-ε, RNG κ-ε).Experimental platform to simulate the airflow and heat transfer at different unsteady turbulence model (standard κ-ε), temperature and velocity variations during cooling. Good agreement between model prediction and measured data was obtained. The root-mean-square error (RMSE) were 1.049 °C,1.033 °C,1.039 °C,1.037 °C,1.014 °C and 1.064 °C for standard κ-ε, RNG κ-ε, Realizableεκ-ε, standard κ-ω and SST κ-ω respectively. There were no significant differences in different turbulence models on simulating the temperature distribution, and it was similar to solve the energy equation on different turbulence models with two eddy viscosity equation. After comparing the accuracy of six two-equation turbulence models, the SST κ-ω model shows more accurate predictions by a comparison of the experimental and simulated results. This research provided reliable method for better understanding and selecting CFD turbulence models to refrigerated transport of fresh fruit.

Olubunmi Popoola et al. (2016) [12] study the influence of turbulence models on the accuracy of CFD analysis of a reciprocating mechanism driven heat loop.

A bellows-type Reciprocating-Mechanism Driven Heat Loops (RMDHL) is a novel heat transfer device that could attain a high heat transfer rate through a reciprocating flow of the working fluid inside the heat transfer device. Although the device has been tested and validated experimentally, analytical or numerical study has not been undertaken to understand its working mechanism and provide guidance for the device design. In an effort to improve earlier numerical models of the RMDHL, different turbulence models for the RMDHL design have been studied and compared with prior experimental results to select the most suitable turbulence modeling techniques. The governing equations have been numerically solved using a CFD solver. For the three-dimensional fluid flow, several turbulence models have been studied for the RMDHL, including Standard, RNG, and Realizable k-ε models, standard and SST k-ω models, transition k-k_l-ω model and the

transition SST model. The results of the simulations have been analyzed and ranked using numerical model calibration template. It was found that the standard k-ω models provided the least accurate results while the RNG-k-ε Model provided the most accurate predictions. It is expected that the results will help improve the accuracy of the work on the RMDHL modeling.

Attila Kiss et al. (2012) [13] studied the sensitivity of a CFD analysis for heat transfer of supercritical water flowing in vertical tubes.

They have taken care about pressure water is considered as the coolant in the primary loop of the presently developed Generation IV Supercritical pressure Water-cooled Reactors (SCWRs), it has been found that CFD codes can calculate the complex thermal hydraulic behavior of supercritical pressure water qualitatively right. The validation of commercial ANSYS CFX code for supercritical pressure water was investigated using priory chosen representative experimental cases. Details of mesh, numerical model and boundary condition sensitivity studies were presented.

T. Bartzanas et al. (2007) [14] realized an analysis of airflow through experimental rural buildings: Sensitivity to turbulence models.

Full-scale experimental data and computational fluid dynamics (CFD) methods are used to determine the accuracy of four different turbulence models [standard k-ε, k-ε renormalisation group (RNG), k-ε realisable, Reynolds Stress Model (RSM)], which are used to describe the turbulent part of air in problems concerning the natural ventilation of buildings.

Airflow and temperature patterns were mapped out in a greenhouse with a tomato crop using a three-dimensional sonic anemometer and a fast-response temperature sensor. The numerical results are compared with the experimental data, and they showed a good agreement, especially when the k-ε RNG turbulence model was used. The computations of the flow field using the different turbulence models showed noticeable differences for computed ventilation rate, air velocity and air temperature confirming the importance of the choice of the closure model for turbulence modeling

Mario Knoll et al. (2020) [15] study the influences of turbulence modeling on particle-wall contacts in numerical simulations of industrial furnaces for thermal particle treatment.

The knowledge of particles that remain in the furnace is important for the efficiency of a thermal particle treatment process. These particles mainly stick to the combustion chamber wall and represent a material loss. To predict the amount of particle-wall contacts in such furnaces, a numerical model based on transient multiphase flow calculations is presented in this work. The proposed model differs from the current state-of-the-art CFD models as

follows: Instead of using the commonly used RANS turbulence models (realizable-k-ε model, Reynolds Stress Model) and steady state calculations, Large Eddy Simulation (LES) of the multiphase flow in the furnace in combination with a type of RANS mesh were performed. Furthermore, the applicability of the LES technique was evaluated by comparing the numerical results to measurements. It was found that the proposed numerical model provides more accurate prediction performance than applying common RANS turbulence models.

CHAPTER 2: TURBULENCE MODELING

Introduction

In this chapter we give a definition of the turbulence and the mesh type. One discuss about the modeling methods used on CFD and a presentation of turbulence modeling. Navier-Stokes equations governing the phenomenon of turbulence are given.

2.1 Introduction to Turbulence

Turbulence is generally considered as one of the unresolved phenomena of physics. This means that there is no model that describes the appearance and maintenance of turbulence in all situations where it appears. Because of the technical importance of turbulence, models based on correlations of particular experimental data have been developed to a large extent. The task to develop a general turbulence model is challenging since turbulence appears almost everywhere: Flows in rivers, oceans and the atmosphere are large scale examples. Flows in pipes, pumps, turbines, combustion processes, in the wake of cars, airplanes and trains are some technical examples. Even the blood flow in the aorta is occasionally turbulent. In fact, one can say that turbulence is the general flow type on medium and large scales whereas laminar flows appear on small scales, and where the viscosity is high. For example, the flow of lubricating oils in bearings is laminar [16].

Fig. 2.1-Turbulence from aircraft swirling clouds below [17].

2.1.1 Turbulence characterization

Turbulence is characterized by the following features:

Turbulent flow tends to occur at higher velocities, low viscosity and at higher characteristic linear dimensions.

- If the Reynolds number is greater than Re > 3500, the flow is turbulent.
- **Irregularity:** The flow is characterized by the irregular movement of particles of the fluid. The movement of fluid particles is chaotic. For this reason, turbulent flow is normally treated statistically rather than deterministically.
- **Diffusivity:** In turbulent flow, a fairly flat velocity distribution exists across the section of pipe, with the result that the entire fluid flows at a given single value and drops rapidly extremely close to the walls. The characteristic which is responsible for

the enhanced mixing and increased rates of mass, momentum and energy transports in a flow is called "diffusivity".

- **Rotationality:** Turbulent flow is characterized by a strong three-dimensional vortex generation mechanism. This mechanism is known as vortex stretching.
- **Dissipation:** A dissipative process is a process in which the kinetic energy of turbulent flow is transformed into internal energy by viscous shear stress [18].

2.1.2 Boundary layer

Boundary layer is the layer of fluid in the immediate vicinity of a bounding surface where the effects of viscosity are significant.
On an aircraft wing the boundary layer is the part of the flow close to the wing, where viscous forces distort the surrounding non viscous flow, the defining characteristic of boundary layer flow is that at the solid walls in figure below, the fluid's velocity is reduced to zero.

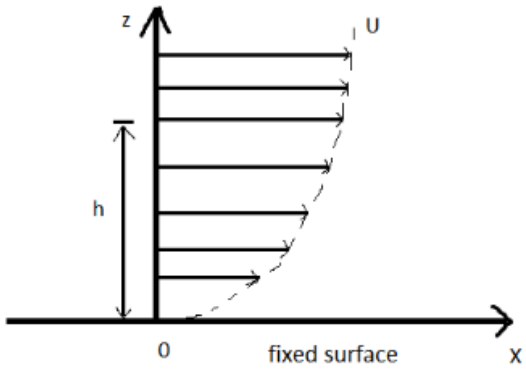

Fig. 2.2 - Boundary layer in fixed surface

2.2 Computational Fluid Dynamics (CFD)

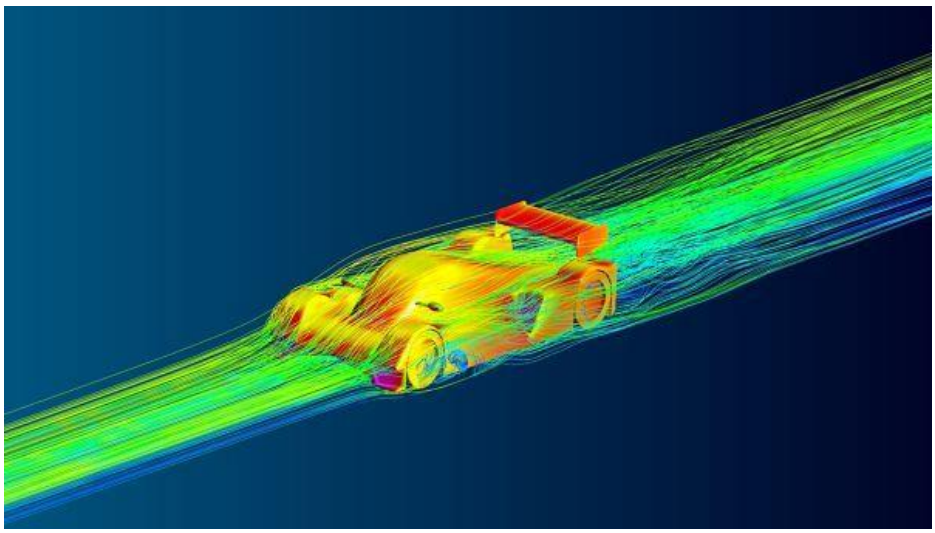

Fig. 2.3 - CFD Simulation of a race car [20].

Computational Fluid Dynamics (CFD) is the use of applied mathematics, physics and computational software to visualize how a gas or liquid flows, as well as how the gas or

liquid affects objects as it flows past. Computational fluid dynamics is based on the Navier-Stokes equations. These equations describe how the velocity, pressure, temperature and density of a moving fluid are related [19].

2.2.1 Application of computational fluid dynamics

As CFD has so many advantages, it is already generally used in industry such as aerospace, automotive, biomedicine, chemical processing, heat ventilation air condition, hydraulics, power generation, sports and marine etc **[1]**.

2.2.2 Navier-Stokes equations

Navier-Stokes equations are the governing equations of Computational Fluid Dynamics. It is based on the conservation law of physical properties of fluid. The principle of conservational law is the change of properties, for example mass, energy, and momentum, in an object is decided by the input and output.

For example, the change of mass in the object is as follows

$$\frac{dM}{dt} = \min - mout \qquad (2.1)$$

If $\dot{M}\text{in} - \dot{M}\text{out} = 0$,we have $\dot{M}\frac{dM}{dt} = 0$ (2.2)

Which means $M = const$

Applying the mass, momentum and energy conservation, we can derive the continuity equation, momentum equation and energy equation as follows [1].

Continuity equation $\frac{d\rho}{dt} + \rho\frac{\partial Ui}{\partial Xi} = 0$ (2.3)

Momentum equation $\underbrace{\rho\frac{\partial Ui}{\partial Xi}}_{\text{I}} + \underbrace{\rho Ui\frac{\partial Uj}{\partial Xj}}_{\text{II}} = \underbrace{-\frac{\partial P}{\partial Xj}}_{\text{III}} \underbrace{-\frac{\partial \tau ij}{\partial xi}}_{\text{IV}} + \underbrace{\rho g_j}_{\text{V}}$ (2.4)

I: Local change with time

II: Momentum convection

III : Surface force

IV : Molecular-dependent momentum exchange (diffusion)

V: Mass force

Energy equation $\rho C_\mu\frac{\partial T}{\partial t} + \rho C_\mu U_i\frac{\partial T}{\partial X_i} = -P\frac{\partial u_i}{\partial x_i} + \lambda\frac{\partial^2 T}{\partial x_i^2} - \tau_{ij}\frac{\partial U_j}{\partial x_i}$ (2.5)

- $\rho C_{\mu} \frac{\partial T}{\partial t}$: Local energy change with time
- $\rho C_{\mu} U_i \frac{\partial T}{\partial X_i}$: Convective term
- $P \frac{\partial u_i}{\partial x_i}$: Pressure work
- $\lambda \frac{\partial^2 T}{\partial x_i^2}$: Heat flux (diffusion)
- $\tau_{ij} \frac{\partial U_j}{\partial x_i}$: Irreversible transfer of mechanical energy into heat

If the fluid is compressible, we can simplify the continuity equation and momentum equation as follows:

Continuity equation $$\frac{\partial U_i}{\partial x_i} = 0 \qquad (2.6)$$

Momentum equation $$\rho \frac{\partial U_i}{\partial t} + \rho U_i \frac{\partial U_j}{\partial X_i} = -\frac{\partial P}{\partial x_j} - \mu \frac{\partial^2 U_j}{\partial x_i^2} + \rho g_j \qquad (2.7)$$

2.3 Meshes types

A mesh divides geometry into many elements. These are used by the CFD solver to construct control volumes. A mesh partitions space into *elements* (or *cells* or *zones*) over which the equations can be solved, which then approximates the solution over the larger domain. Element boundaries may be constrained to lie on internal or external boundaries within a model [21].

Grid/Mesh

A mesh divides geometry into many elements. These are used by the CFD solver to construct control volumes [21].

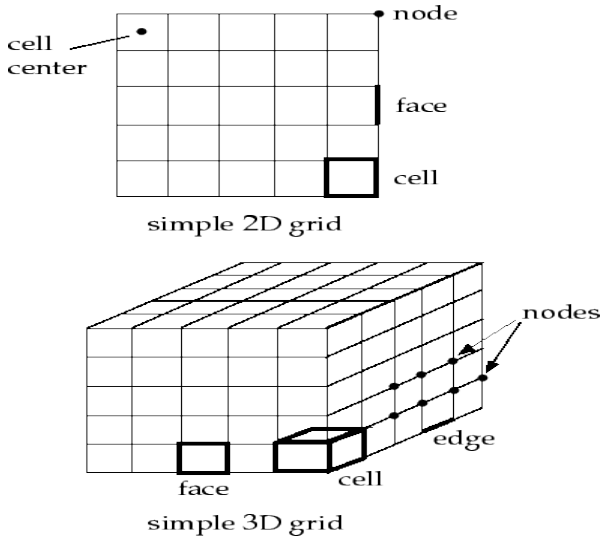

Fig.2.4 : Mesh components [22].

Terminology:

• Cell = control volume into which domain is broken up.

• Node = grid point.
• Cell center = center of a cell.
• Edge = boundary of a face.
• Face = boundary of a cell.
• Zone = grouping of nodes, faces, cells

The shapes of control volumes depend on the capabilities of the solver. Structured-grid codes use quadrilaterals in 2D and hexahedrons in 3D flows. Unstructured-grid solvers often use triangles (2D) or tetrahedron (3D), but newer codes can use arbitrary polyhedrons [21].

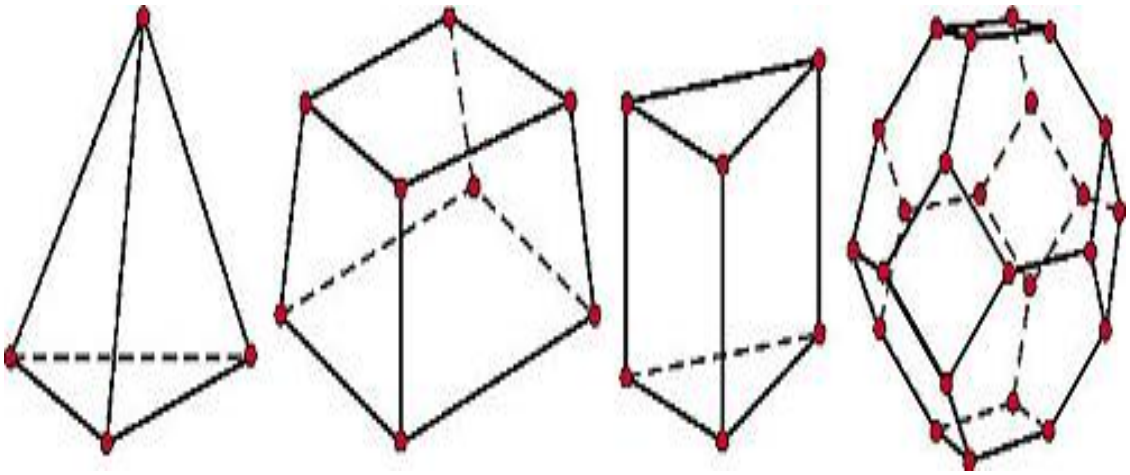

Fig.2.5 -Cell Type [22].

2.3.1 Structured mesh

A structured mesh is defined as a mesh where the inner nodes have the same number of elements around them [23].
Structured grids are identified by regular connectivity. The possible element choices are quadrilateral in 2D and hexahedra in 3D.

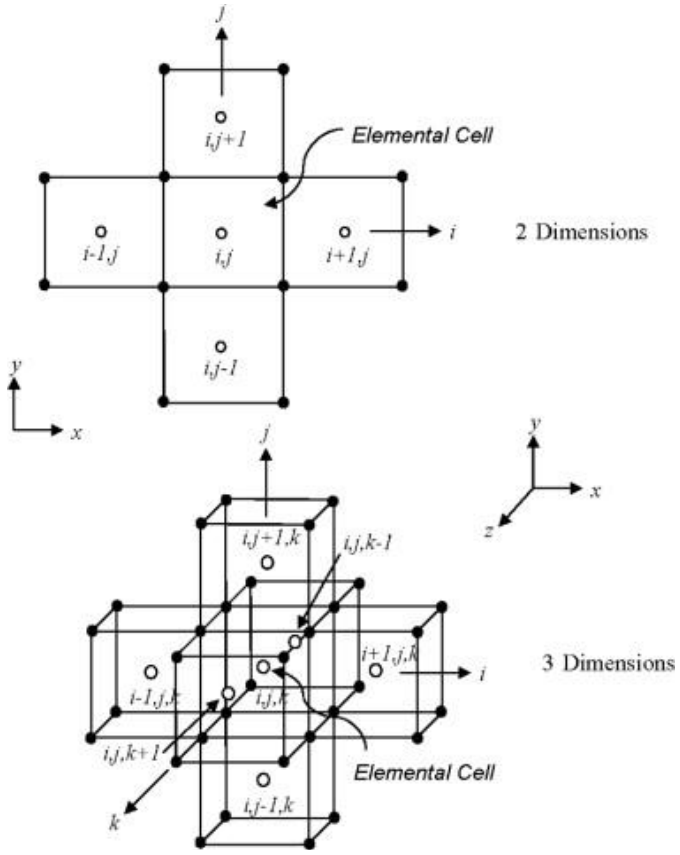

Fig. 2.6 - Nodal indexing of elemental cells in two and three dimensions for a structured mesh [24].

2.3.2 Unstructured mesh

An unstructured grid is identified by irregular connectivity. It cannot easily be expressed as a two-dimensional or three-dimensional array in computer memory. This allows for any possible element that a solver might be able to use. Compared to structured meshes, this model can be highly space inefficient since it calls for explicit storage of neighborhood relationships. These grids typically employ triangles in 2D and tetrahedral in 3D [25].

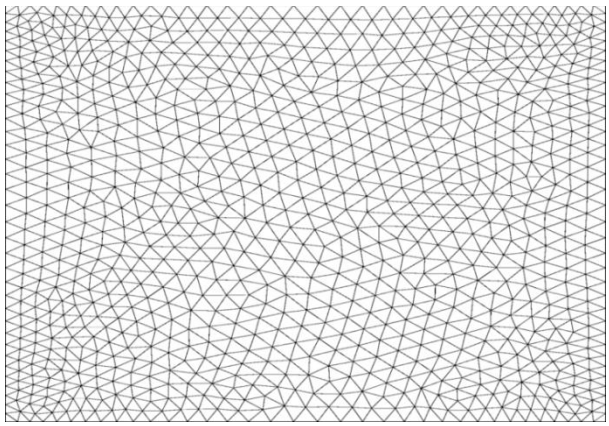

Fig. 2.7 - Unstructured mesh for computations of lid-driven cavity flows [26]

2.3.3 Mixed mesh

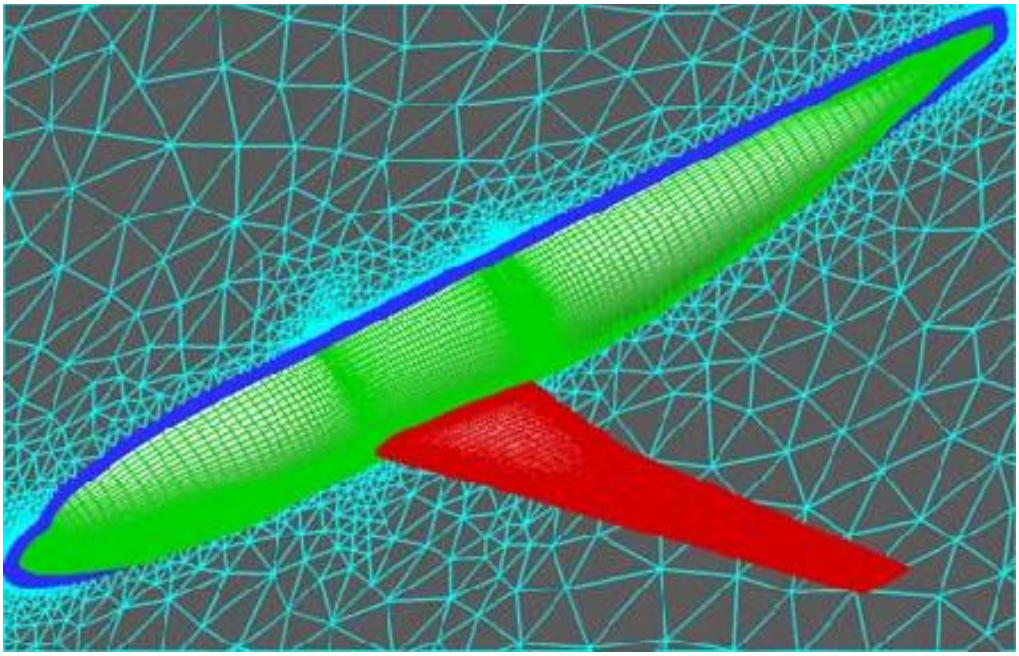

Fig. 2.8 - Mixed mesh. [27]

A hybrid grid contains a mixture of structured portions and unstructured portions. It integrates the structured meshes and the unstructured meshes in an efficient manner. Those parts of the geometry that are regular can have structured grids and those that are complex can have unstructured grids. These grids can be non-conformal which means that grid lines don't need to match at block boundaries [28].

2.4 Modeling methods

2.4.1 Direct Numerical Simulation (DNS)

Direct numerical simulation (DNS) is used to solve instantaneous Navier–Stokes equations, resolving all scales, down to Kolmogorov dissipation scales, without using any models. It can give the most accurate results, with high spatial and temporal resolution, which cannot even be given by measurements.

However, its computer requirements are extremely high, and increase rapidly with Reynolds number. Therefore, its application is limited to low-Reynolds number flows and small-size computation domains.

Therefore, currently, DNS cannot be used to simulate practical high-Reynolds-number complex flows. However, the DNS database can be used to validate the RANS and LES-SGS models. Since there are no closure models in DNS, it only has highly accurate numerical methods and proper boundary conditions. The adopted numerical methods include spectral method, pseudo-spectral method, and finite difference method with a highly accurate

compact difference scheme. DNS needs periodic boundary conditions at the inlet and walls. The Kolmogorov scale is determined by [29].

$$\eta = \left(\nu^3/\varepsilon\right)^{1/4} \quad (2.8)$$

where ν is the kinematic viscosity and ε is the dissipation rate of turbulent kinetic energy. It is known that

$$\varepsilon \approx (u')^3/L \quad (2.9)$$

Where u' is the RMS of fluctuation velocity, and L is the integral scale. $L = \frac{K^{3/2}}{\varepsilon}$

The three-dimensional grid number should be at least

$$N = (N_X)^3 = (Re_L)^{9/4} \quad (2.10)$$

That for Re_L = 6000, the required grid number should be 2×10^9, and the computation time 20 months.

2.4.2 Large Eddy Simulation (LES).

The larger eddies obtain their kinetic energy from the bulk fluid energy, contain most of the turbulent kinetic energy (~80%), transfer kinetic energy to the smaller eddies by stretching and breaking them up ("cascading"), and are responsible for the majority of the diffusive processes involving mass, momentum, and energy. For these reasons, the simulation of large eddies is highly desirable (LES).

As expected, the LES methodology divides the simulation into two areas. One portion calculates the velocity field of the larger eddies, thereby resolving their behavior explicitly, while the subgrid portion represents the smaller eddies, which are modeled (approximated).

Conceptually shows that LES resolves integral and Taylor eddies up to a user or mesh defined minimum eddy size Δ, while direct numerical simulation (DNS) resolves the integral, Taylor, and Kolmogorov eddies (i.e., DNS calculates all scales). In this context, the scale Δ determines the minimum size for which eddies will be resolved, thereby acting as a filter for the subgrid scale (SGS), whereby eddies smaller than Δ are modeled [30].

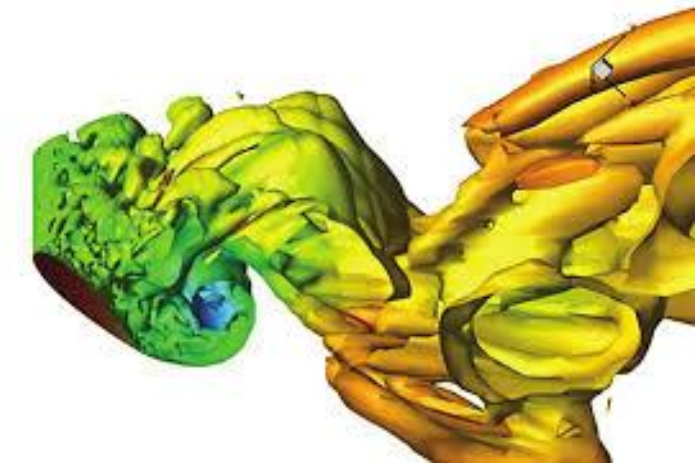

Fig.2.9 - L.E.S Simulation [31]

2.4.3 Reynolds Averaged Navier-Stokes (RANS)

Reynolds Averaged Navier-Stokes (RANS) turbulence models are usually concerned with modeling the Reynolds stress tensor [32].

The idea behind the equations is Reynolds decomposition, whereby an instantaneous quantity is decomposed into its time-averaged and fluctuating quantities, an idea first proposed by Osborne Reynolds. The RANS equations are primarily used to describe turbulent flows.

The basic tool required for the derivation of the RANS equations from the instantaneous Navier–Stokes equations is the Reynolds decomposition. (like velocity $\boldsymbol{u}$) into the mean (time-averaged) component ($\overline{\boldsymbol{u}}$) and the fluctuating component ($\boldsymbol{u}'$)[33].

$$\boldsymbol{u} = \overline{\mathbf{u}} + \boldsymbol{u}'$$

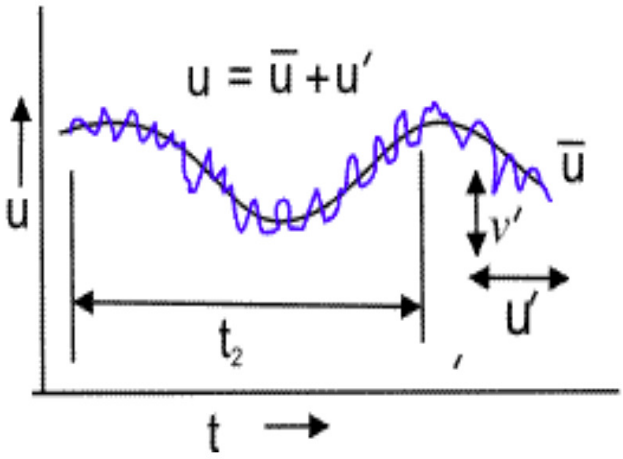

Fig. 2.10 - Diagram of the Reynolds decomposition [34].

The incompressible Navier-Stokes equations in conservation form are

$$\frac{\partial u_i}{\partial x_i} = 0 \quad (2.11)$$

$$\rho \frac{\partial u_i}{\partial t} + \rho \frac{\partial}{\partial x_j}(u_j u_i) = -\frac{\partial p}{\partial x_i} + \frac{\partial}{\partial x_j}(2\mu s_{ij}) \quad (2.12)$$

Where the strain-rate tensor s_{ij} is given by

$$s_{ij} = \frac{1}{2}\left(\frac{\partial u_i}{\partial x_j} + \frac{\partial u_j}{\partial x_i}\right) (2.13)$$

By the application of Eq. (2.11), the equations of motion can be written as

$$\rho \frac{\partial u_i}{\partial t} + \rho u_j \frac{\partial u_i}{\partial x_j} = -\frac{\partial p}{\partial x_i} + \mu \frac{\partial^2 u_i}{\partial x_i \partial x_j} \quad (2.14)$$

In turbulent flows, the field properties become random functions of space and time. Hence, the field variables u_i and p must be expressed as the sum of mean and fluctuating parts as

$$u_i = \bar{u} + u_i^{'} \ , \ p = \bar{p} + p' \quad (2.15)$$

Where the mean and fluctuating parts satisfy

$$\overline{u}_i = U_i \ , \overline{u}_i^{'} = 0$$

$$\overline{p} = P \ , \overline{p}^{'} = 0$$

With the bar denoting the time average, we insert Eq. (2.15) into (2.11)-(2.12) and take the time average to arrive at the Reynolds-averaged Navier-Stokes (RANS) equations

$$\frac{\partial U_i}{\partial x_i} = 0 \quad (2.16)$$

$$\rho \frac{\partial U_i}{\partial t} + \rho \frac{\partial}{\partial x_j}\left(U_i U_j\right) = -\frac{\partial p}{\partial x_i} + \frac{\partial}{\partial x_j}(2\mu s_{ij} - \rho \overline{u_i^{'} u_j^{'}}) \quad (2.17)$$

Where Sij is the mean strain-rate tensor

$$S_{ij} = \frac{1}{2}\left(\frac{\partial U_i}{\partial x_j} + \frac{\partial U_j}{\partial x_i}\right) \quad (2.18)$$

The quantity $\tau_{ij} = -\overline{u_i^{'} u_j^{'}}$ is known as the Reynolds stress tensor which is symmetric and thus has six components. By the application of (2.16) Eq. (2.17) can then be expressed as

$$\frac{\partial U_i}{\partial t} + U_j \frac{\partial U_i}{\partial x_j} = -\frac{\partial p}{\partial x_i} + v \frac{\partial^2 U_i}{\partial x_i \partial x_j} - \frac{\partial \overline{u_i^{'} u_j^{'}}}{\partial x_j} \quad (2.19)$$

And now we decomposing the instantaneous proportions into mean and fluctuating parts, then we have three unknown quantities.

For that we need to close the system, we must find enough equation to solve for our unknown and in what follows we describe the turbulence models [33].

2.5 Turbulence models

2.5.1. Boussinesq approximation

The Reynolds-averaged approach to turbulence modeling requires that the Reynolds stresses in Equation (2.19) be appropriately modeled. A common method employs the Boussinesq hypothesis to relate the Reynolds stresses to the mean velocity gradients [35].

$$-\rho\overline{u_i'u_j'} = 2v_T s_{ij} - \frac{2}{3}k\delta_{\mathrm{ij}} \quad (2.20)$$

Where the turbulence kinetic energy, k, is defined as

$$k = \frac{1}{2}\overline{u_i'u_i'} \quad (2.21)$$

And v_T is the kinetic eddy viscosity assumed as an isotropic scalar quantity-which is not strictly true –so that the term "approximation" is appropriate.

2.5.2 Spalart-Allmaras model

In Spalart-Allmaras model, the turbulence kinetic energy is not calculated, the last term in Equation (2.22) is ignored when estimating the Reynolds stresses

$$-\overline{u_i'u_j'} = 2v_T S_{ij} \quad (2.22)$$

The model includes eight closure coefficients and three closure functions. Its defining equations are as follows:

$$v_T = \overline{v}f_{v1}, \quad f_{v1} = \frac{X^3}{X^3+C_{v1}^3} \quad ,X = \frac{\overline{v}}{v} \quad (2.23)$$

v: is the molecular viscosity

$\overline{v}$: obeys the transport equations

$$\frac{\partial\overline{v}}{\partial t} + U_j\frac{\partial\overline{v}}{\partial x_j} = C_{b1}\overline{S}\overline{v} + \frac{1}{6}\frac{\partial}{\partial x_k}\left[(v+\overline{v})\frac{\partial\overline{v}}{\partial x_k}\right] + \frac{C_{b2}}{\delta}\frac{\partial\overline{v}}{\partial x_k}\frac{\partial\overline{v}}{\partial x_k} - C_{w1}f_w\left[\frac{\overline{v}}{d}\right]^2 \quad (2.24)$$

Where

$$C_{b1} = 0{,}1355\ , \qquad C_{b2} = 0.622\ , C_{v1} = 7.1\ , \delta = {}^{2}/_{3}$$

$$C_{w1} = \frac{C_{b1}}{k^2} + \frac{(1 + C_{b2})}{\sigma}\ , \qquad f_w = g\left[\frac{1 + C_{w3}^6}{g^6 + C_{w3}^6}\right]^{1/6}, \qquad g = r + C_{w2}(r^6 - r)$$

$$r = \frac{\overline{v}}{\overline{S}k^2 d^2}, \overline{S} = S + \frac{\overline{v}}{k^2 d^2} f_{v2}, S = \sqrt{\Omega_{ij}\Omega_{ij}}$$

The tensor $\Omega_{ij} = \frac{1}{2}\left({}^{\partial U_i}/_{\partial x_j} - {}^{\partial U_j}/_{\partial x_i}\right)$ is the rotation tensor and d is distance from the closest surface [27].

2.5.3 k-ε model

A k-epsilon model is based on the Bousinesq concept (1977). It is the most common model used in Computational Fluid Dynamics (CFD). It is a two equation model that gives a general description of turbulence by means of two transport equations (PDEs). The model transport equation for k is derived from the exact equation, while the model transport equation for ε was obtained using physical reasoning and bears little resemblance to its mathematically exact counterpart.

In the derivation of the $k - \varepsilon$ model, it was assumed that the flow is fully turbulent, and the effects of molecular viscosity are negligible. The standard $k - \varepsilon$ model is therefore valid only for fully turbulent flows. This model is only applicable far enough of the walls. For this reason, it is often associated with a wall law that avoids the resolution heavy on the balance sheet equations up to that wall [36].

Kinetic eddy viscosity:

$$v_{t=}\rho v_t = \rho C_\mu \frac{K^2}{\varepsilon} \quad (2.25)$$

Turbulence kinetic energy :

$$\frac{\partial k}{\partial t} + U_j \frac{\partial k}{\partial x_j} = \tau_{ij}\frac{\partial U_i}{\partial x_j} - \varepsilon + \frac{\partial}{\partial x_j}\left[(v + v_T/\delta_k)\frac{\partial k}{\partial x_j}\right] \quad (2.26)$$

Specific dissipation rate:

$$\frac{\partial \varepsilon}{\partial t} + U_j \frac{\partial \varepsilon}{\partial x_j} = C_{\varepsilon 1}\frac{\varepsilon}{k}\tau_{ij}\frac{\partial U_i}{\partial x_j} - C_{\varepsilon 2}\frac{\varepsilon^2}{k} + \frac{\partial}{\partial x_j}\left[(v + v_T/\delta_\varepsilon)\frac{\partial \varepsilon}{\partial x_i}\right] \quad (2.27)$$

Closure coefficients and relations:

C_μ	$C_{\varepsilon 1}$	$C_{\varepsilon 2}$	δ_k	δ_ε
0.09	1.44	1.92	1	1.3

Table 2.1 - Values of k-ε model constant

It is essential to know that k-ε model is applicable to flows at high Reynolds number [37].

2.5.4 k-ω model

The K-omega model is one of the most commonly used turbulence models, the k–omega (*k*–ω) turbulence model is a common two-equation turbulence model, that is used as a closure for the Reynolds-averaged Navier–Stokes equations (RANS equations). The model attempts to predict turbulence by two partial differential equations for two variables, *k* and ω, with the first variable being the turbulence kinetic energy (*k*) while the second (ω) is the specific rate of dissipation (of the turbulence kinetic energy *k* into internal thermal energy) [38].

Kinetic eddy viscosity:

$v_T = {}^{k}/_{\omega}$ (2.28)

Turbulence kinetic energy:

$$\frac{\partial k}{\partial t} + U_j \frac{\partial k}{\partial x_j} = \tau_{ij} \frac{\partial U_i}{\partial x_j} - \beta^* k\omega + \frac{\partial}{\partial x_j}\left[(v + \delta^* vT)\frac{\partial k}{\partial x_j}\right] \quad (2.28)$$

Specific dissipation rate:

$$\frac{\partial \omega}{\partial t} + U_j \frac{\partial \omega}{\partial x_j} = \alpha \frac{\omega}{\mathrm{k}} \tau_{ij} \frac{\partial U_i}{\partial x_j} - \beta\omega^2 + \frac{\partial}{\partial x_j}\left[(v + \delta v_T)\frac{\partial \omega}{\partial x_j}\right] (2.29)$$

K: kinetic energy of turbulence

W: specific dissipation rate, it is defined by $\omega = \frac{\varepsilon}{k}$

U: average fluid velocity

Closure Coefficients and Relations:

$$\alpha = \frac{13}{25}, \beta = \beta_0 f_\beta \quad , \beta^* = \beta_0^* f_{\beta^*} \quad , \quad \alpha = \frac{1}{2}, \qquad \delta^* = \frac{1}{2}$$

$$\beta_0 = \frac{9}{125} \quad , \quad f_\beta = \frac{1 + 70x_\omega}{1 + 80x_\omega}$$

$$\beta_0^* = \frac{9}{100} \quad , \quad f_{\beta^*} = \begin{cases} 1, x_k \leq 0 \\ \frac{1+680x_k^2}{1+400x_K^2}, \quad x_k > 0 \end{cases}$$

$$x_k = \frac{1}{\omega^3}\frac{\partial k}{\partial x_i}\frac{\partial \omega}{\partial x_j}$$

2.5.5 k-ω SST modeling

The SST k-ω turbulence model (Shear Stress Transport - Menter 1993) is a two-equation eddy-viscosity model which has become very popular. The shear stress transport (SST) formulation combines the best of two worlds. The use of a k-ω formulation in the inner parts of the boundary layer makes the model directly usable all the way down to the wall through the viscous sub-layer, hence the SST k-ω model can be used as a Low-Re turbulence model without any extra damping functions. The SST formulation also switches to k-ε behavior in the free-stream and thereby avoids the common k-ω problem that the model is too sensitive to the inlet free-stream turbulence properties. Authors who use the SST k-ω model often merit it for its good behavior in adverse pressure gradients and separating flow. The SST k-ω model does produce a bit too large turbulence levels in regions with large normal strain, like stagnation regions and regions with strong acceleration. This tendency is much less pronounced than with a normal k-ε model though [39].

Turbulence kinetic energy

$$\frac{\partial k}{\partial x} + U_j\frac{\partial k}{\partial x_j} = P_k - \beta^* k\omega + \frac{\partial}{\partial x_j}\left[(v + \delta_k v_T)\frac{\partial k}{\partial x_j}\right] \quad (2.30)$$

Specific dissipation rate

$$\frac{\partial \omega}{\partial t} + U_j\frac{\partial \omega}{\partial x_j} = \alpha S^2 - \beta\omega^2 + \frac{\partial}{\partial x_i}\left[(v + \delta_\omega v_T)\frac{\partial \omega}{\partial x_i}\right] + 2(1 - F_1)\delta_{\omega^2}\frac{1}{\omega}\frac{\partial k}{\partial x_i}\frac{\partial \omega}{\partial x_i} (2.31)$$

F1 (Blending Function)

$$F_1 = \tan h\left\{\left\{min\left[max\left(\frac{\sqrt{k}}{\beta^*\omega y}, \frac{500v}{y^2\omega}\right), \frac{4\delta\omega^2 k}{CD_{k\omega}y^2}\right]\right\}^4\right\} (2.32)$$

Note: F1 = 1 inside the boundary layer and 0 in the free stream. And y is the closest distance to the wall.

$$CD_{k\omega} = max\left(2\rho\delta_{\omega^2}\frac{1}{\omega}\frac{\partial k}{\partial x_i}\frac{\partial \omega}{\partial x_i}, 10^{-10}\right) (2.33)$$

Kinematic eddy viscosity

$$v_T = \frac{a_1 k}{max(a_1\omega, SF_2)} \quad (2.34)$$

s: is the invariant measure of the deformation rate.

F2 (second blending function)

$$F_2 = \tan h\left[\left[\max\left(\frac{2\sqrt{k}}{\beta^*\omega y}, \frac{500v}{y^2\omega}\right]^2\right]\right] \quad (2.35)$$

P_K (Production limiter)

$$P_k = min\left(\tau_{ij}\frac{\partial U_i}{\partial x_j}, 10\beta^* k\omega\right) \quad (2.36)$$

All constants are calculated by mixing the corresponding constants of the model $k-\varepsilon$ and model $k-\omega$ by $\alpha = \alpha_1 F + \alpha_2(1-F)$[40]

β^*	α_1	β_1	δ_{k1}	$\delta_{\omega 1}$	α_2	β_2	δ_{k2}	$\delta_{\omega 2}$
0.09	$\frac{5}{9}$	$\frac{3}{40}$	0.85	0.5	0.44	0.0828	1	0.856

Table 2.2 - Values of $K-\omega SST$ model constants

2.6 Finite volume method

The finite volume method (FVM) is a method for representing and evaluating partial differential equations in the form of algebraic equations. In the finite volume method, volume integrals in a partial differential equation that contain a divergence term are converted to surface integrals, using the divergence theorem. These terms are then evaluated as fluxes at the surfaces of each finite volume. Because the flux entering a given volume is identical to that leaving the adjacent volume, these methods are conservative. Another advantage of the finite volume method is that it is easily formulated to allow for unstructured meshes. The method is used in many computational fluid dynamics packages. "Finite volume" refers to the small volume surrounding each node point on a mesh [41].The principle of discretization can be illustrated by considering the transport equation for a scalar quantity ϕ, valid for all flow equations, in steady state[42].

$$\oint_A (\rho\phi\vec{v})\, d\vec{A} = \oint_A \left(\Gamma\phi\overrightarrow{grad}\phi\right) d\vec{A} + \int_{VC} S_\phi dV \quad (2.37)$$

With

ρ:Fluiddensity

$\vec{v}$: Velocity vector$\left(\vec{v} = v_x\vec{\imath} + v_y\vec{\jmath}\right)$

$\overrightarrow{A}$:Surfacearea vector

Γ_ϕ: Diffusion coefficient of the quantityϕ.

$\overrightarrow{grad}\phi$: Gradient of ϕ.

S_ϕ: Source term (the source of Φ per unit of volume).

Equation (2) is applied to each control volume in the computational domain

(Field of study or analysis), the discretization of this equation gives:

$$\sum_{f}^{N_{faces}} \rho_f \, v_f \phi_f A_f = \sum_{f}^{N_{faces}} \Gamma\phi(\nabla\phi)_n A_f + S_\phi V$$

With

N_{faces}: Number of sides of the control volume.

ϕ_f: Convection Transfer value cross the interface Φ.

v_f: Mass flow through the interface f.

$\boldsymbol{A_f}$: Interface area f(| $\vec{\boldsymbol{A}}$ |=|$\boldsymbol{A_x\vec{\imath}}$+$\boldsymbol{A_y\vec{\jmath}}$| en 2D)

$\left(\vec{\nabla}\phi\right)_n$: Normal$\vec{\nabla}$ Φ value at the interface

V: control volume

Conclusion

In this chapter we have identified the equation of incompressible turbulent flow, and the system of equations governing the phenomenon of turbulence. These equations based on the Reynolds decomposition method (RANS) and we give a presentation on the finite volume method, which used to solve this system

CHAPTER 3: NUMERICAL RESOLUTION AND FREE SOFTWARE

Introduction

In what follows, we give a presentation about the open source and free CFD software and, its advantages and how it works in numerical calculation (code_Saturn, GMSH, and EnSight). And we talked about the free software Grace which is 2D graph plotting tool, which we will use in our research and we gave a definition we provided the definition of the boundary condition.

3.1 Presentation of GMSH

Gmsh is a finite-element mesh generator developed by Christophe Geuzaine and Jean-François Remacle. Released under the GNU General Public License, Gmsh is free software.

Gmsh contains 4 modules: for geometry description, meshing, solving and post-processing. Gmsh supports parametric input and has advanced visualization mechanisms. Since version 3.0, Gmsh supports full constructive solid geometry features, based on Open Cascade Technology [43].

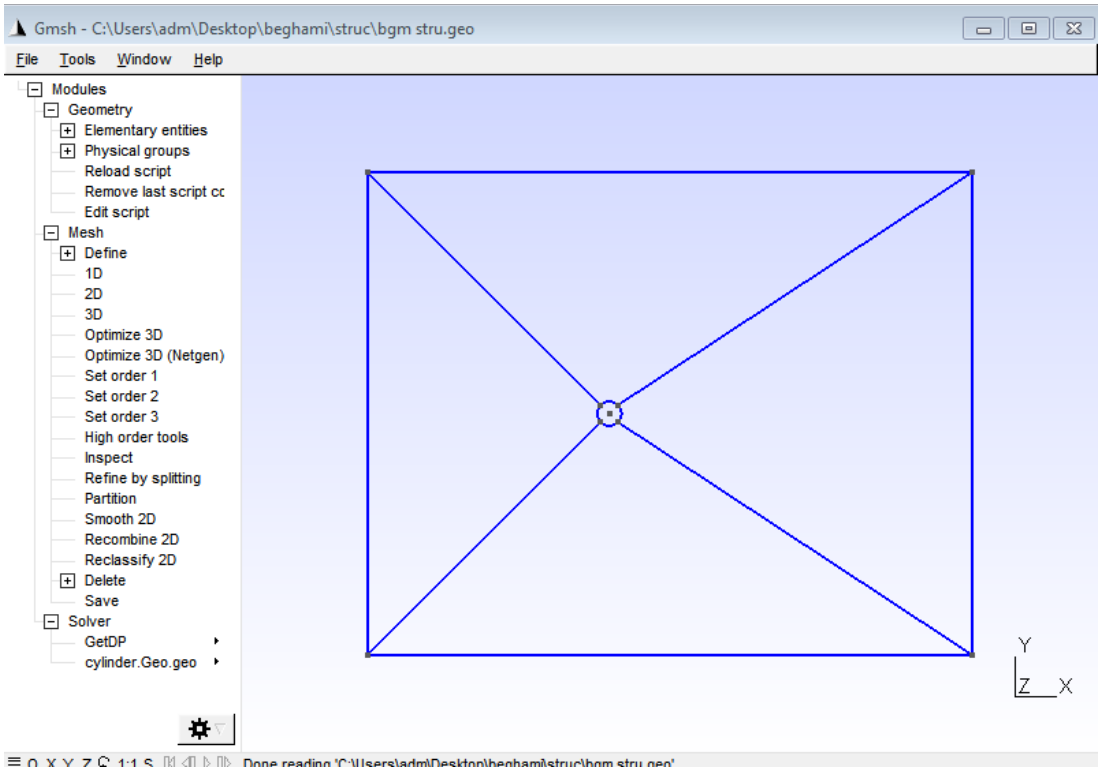

Fig. 3.1 - Gmsh graphical interface.

3.2 Presentation of Code_Saturne

Code_Saturne is the free, open-source software developed and released by EDF to solve computational fluid dynamics (CFD) applications.

It solves the Navier-Stokes equations for 2D, 2D-axisymmetric and 3D flows, steady or unsteady, laminar or turbulent, incompressible or weakly dilatable, isothermal or not, with scalars transport if required.

Several turbulence models are available, from Reynolds-Averaged models to Large-Eddy Simulation models. In addition, a number of specific physical models are also available as modules: gas, coal and heavy-fuel oil combustion, semi-transparent radiative transfer, particle-tracking with Lagrangian modeling, Joule effect, electrics arcs, weakly compressible flows, atmospheric flows, rotor/stator interaction for hydraulic machines[44].

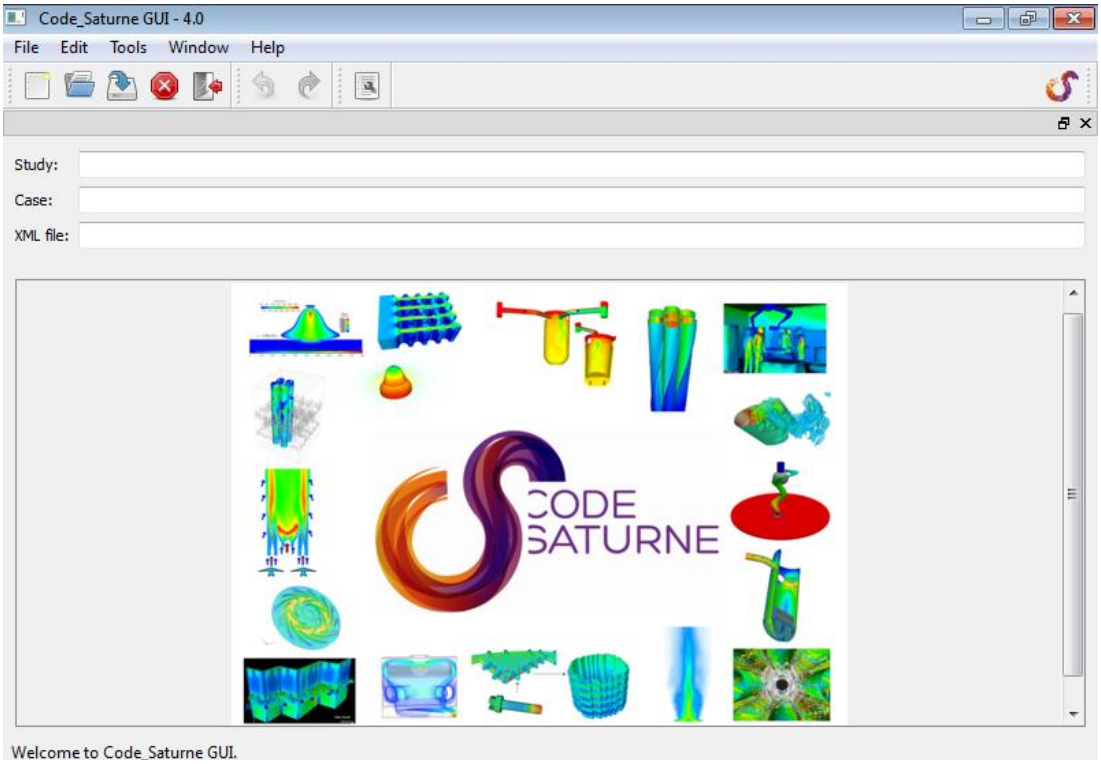

Fig. 3.2-Code_Satunre graphical interface

3.2.1 Numerical method in Code_saturne

Discretization

Code_Saturne is based on a co-located finite volume approach that handles meshes with any type of cell (tetrahedral, hexahedral, prismatic, pyramidal, polyhedral…) and any type of grid structure (unstructured, block structured, hybrid, conforming or with hanging nodes…).
Code_Saturne can solve flows in steady or unsteady mode. It uses a theta scheme for the time discretization

Velocity-pressure coupling

*Code_Saturne*uses a fractional step method, similar to SIMPLEC.

- Velocity prediction: Solve the momentum equation with an explicit pressure gradient and obtain a predicted velocity
- Pressure correction: Use the continuity equation to enforce mass conservation
- Update velocity field using ∇P

After the velocity has been updated, the resolution of turbulent variables and scalars is done according to their time scheme.
Rhie & Chow interpolation is used when solving the pressure to avoid oscillations

Linear system resolution

Code_Saturne has different ways of solving the linear system:

- Jacobi (default for velocity, temperature, turbulent variables, passive scalars)
- Algebraic multigrid (default for pressure)
- Conjugate gradient
- Stabilized bi-conjugate gradient (BI-CGSTAB)[44]

3.3 Boundary conditions

In mathematics, in the field of differential equations, a boundary value problem is a differential equation together with a set of additional constraints, called the boundary conditions. A solution to a boundary value problem is a solution to the differential equation which also satisfies the boundary conditions [45].

Boundary conditions are required in at least three main cases:

- Calculation of the convection terms (first order derivative in space) at the boundary: the code uses a mass flux at the boundary and requires the value of the convected variable when the flow is entering into the domain (or more general wave relations in the sense of the characteristic curves of the system entering the domain).
- Calculation of the diffusion terms (second order derivative in space): the code needs a method to determine the value of the first order spatial derivatives at the boundary; these define e.g. the stresses or the thermal fluxes at the wall.
- Calculation of the cell gradients: the variables at the boundary faces allow the code to define the gradient inside the cell connected to the boundary (e.g. the pressure gradient or the transpose gradient terms in the stress-strain relation).

These considerations only concern the computational field variables (velocity, pressure, Reynolds tensor, scalars solution of an advection-diffusion equations etc.). For these variables 1, the user has to define the boundary conditions at every boundary face. The boundary conditions could be of Neumann type (when the flux is imposed) or Dirichlet type (when the value of the field variable is prescribed), or mixed type, also called Robin type (when a combination linking the field variable to its derivative flux is imposed).

A particular treatment on symmetry boundaries is also performed for vectors and tensors whereas a symmetry boundary is equivalent to an homogeneous Neumann condition (zero normal gradient) for scalar fields ,The physics model that the user wishes to apply needs to be translated into pairs of coefficients entering the linear system of equations that the code will solve. For any variable Y for every boundary faces f_b these coefficients are:[45]

$\left(A_{fb}^{g}, B_{fb}^{g}\right)$ Used by the gradient operator and by the advection operator. The value at the boundary face f_b of the variable Y is then defined as:

$$Y_{fb} = A_{fb}^{g} + B_{fb}^{g} Y_{I'}$$

$\left(A_{ib}^{f}, B_{ib}^{f}\right)$ Used by the diffusion operator. The value at the boundary faces f_b of the diffusive flux q_{ib} of the variable:

$$q_{ib} = \frac{D_{ib}\left(K_{fb}, Y\right)}{|S| f_b} = -\left(A_{ib}^{f} + B_{ib}^{f} Y_{I'}\right)$$

Note that the diffusive boundary coefficients are oriented, which means that they are such that if $D_{ib}\left(K_{fb}; Y\right)$) is positive, this flux is gained by $Y_{I'}$.

3.3.1Standard user boundary conditions:

The user generally gives standard boundary conditions, which are:

Outlet: it corresponds to a homogeneous Neumann boundary condition on all the transported variables. For the pressure field, a Dirichlet boundary condition which is expected to mimic $\frac{\partial^2 P}{\partial n \partial \tau}$=0 for any vector ($\tau$) τ parallel to the outlet face. This condition means that the pressure profile does not vary in the normal direction of the outlet. Warning: if the outgoing mass-flux is negative, $i.e.$ if the outlet becomes an inlet, then the mass-flux is clipped to zero. Moreover, since the pressure field is defined up to a constant, it is fixed to a reference pressure P_0 at an arbitrary chosen outlet boundary face. The user can choose another desired face where a Dirichlet on pressure is prescribed.

Free inlet/outlet: it corresponds to the standard outlet when the flow is outgoing but to a free inlet when the flow is ingoing. The Bernoulli relationship is used to derive a boundary condition on the pressure increment to couple velocity and pressure at these free inlet faces. Note that no clipping on the velocity is imposed. The same boundary conditions as for outlet on the other variables is imposed.

Walls: This particular treatment will be detailed in the following sections. For the velocity, the aim is to transform the Dirichlet boundary condition (the velocity at the wall is equal to zero or the velocity of a moving wall) into a Neumann boundary condition where the wall shear stress is imposed function of the local flow velocity and the turbulence characteristics. A similar treatment using wall functions is done on every transported variable if this variable is prescribed. The boundary condition on the pressure field is a homogeneous Neumann by default, or alternatively an extrapolation of the gradient.

Symmetries: This condition corresponds to a homogeneous Neumann for the scalar fields (e.g. the pressure field or the temperature field). For vectors, such as the velocity, it corresponds to impose a zero Dirichlet on the component normal to the boundary, and a homogeneous Neumann on the tangential components. Thus, this condition couples the vector components if the symmetry faces are not aligned with the reference frame. The boundary condition for tensors, such as the Reynolds stresses, will be detailed in the following sections [46].

Basic Dirichlet boundary conditions

Imposing a basic Dirichlet condition Y_{fb}^{imp} on a boundary face f_b is translated into:

$$\begin{cases} A_{fb}^{g} = Y_{fb}^{imp}, \\ B_{fb}^{g} = 0, \end{cases} \begin{cases} A_{ib}^{f} = -h_{int} + Y_{fb}^{imp}, \\ B_{ib}^{f} = h_{int}\ , \end{cases}$$

The term h_{int} is an internal coding coefficient (automatically provided by the code) similar to an exchange coefficient.

Neumann boundary conditions

Imposing a Neumann condition D_{ib}^{imp} on a boundary face f_b is translated into

$$\begin{cases} A_{fb}^{g} = -\dfrac{D_{ib}^{imp}}{h_{int}}, \\ B_{fb}^{g} = 1, \end{cases} \begin{cases} A_{ib}^{f} = D_{ip}^{imp}, \\ B_{ib}^{f} = 0. \end{cases}$$

3.4Presentation of EnSight

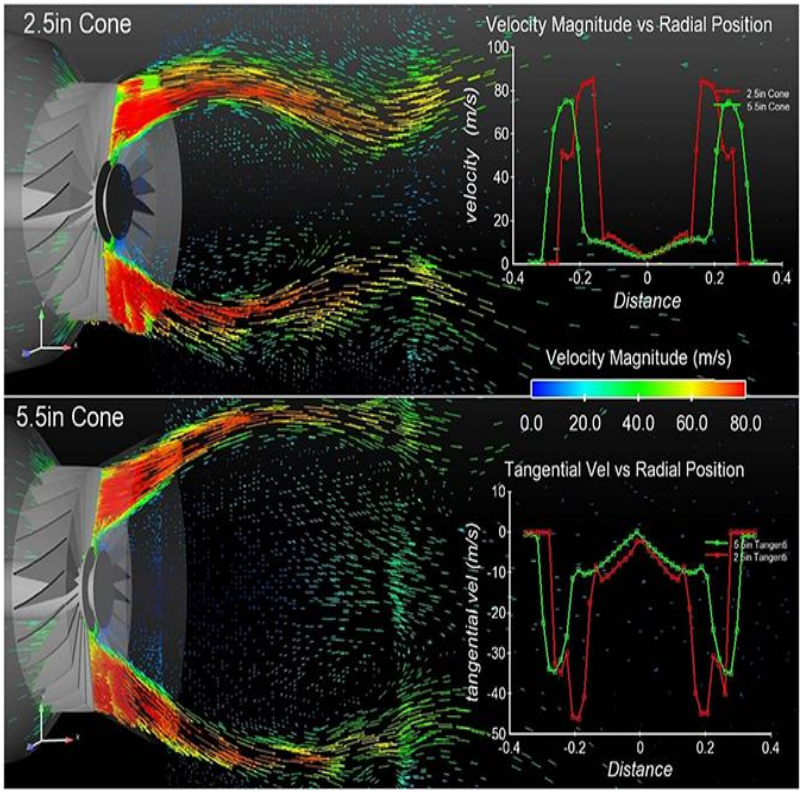

Fig. 3.3-EnSight is used to embed charts of velocity versus radial position over flow analysis results [47].

Analyze, visualize and communicate your simulation data with EnSight. Engineers use this powerful, general purpose post-processing tool to gain new design insights and then clearly and effectively sell their recommendations. Flexible EnSight can read and visualize data from most simulation tools.

EnSight is more than the leading post-processor and visualization software program: It is a data fusion program. It consolidates data from multiple engineering simulations and other sources to help explore and explain complex systems and processes. It handles simulation data from a wide range of physics from fluids, structures, particles, crash and more. With

EnSight, you can create and communicate the best looking, clear, highest resolution simulation results on datasets that were previously thought to be too big to handle [48].

3.5 Presentation of Paraview

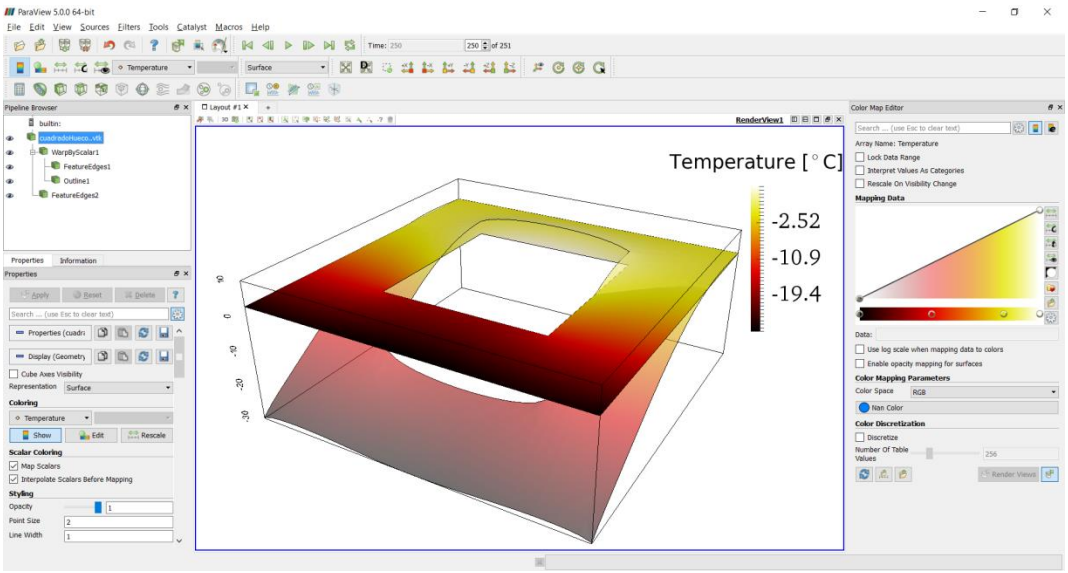

Fig. 3.4 – Paraview graphical interface [49]

ParaView is an open-source, multi-platform data analysis and visualization application. Paraview is known and used in many different communities to analyze and visualize scientific data sets [49].It can be used to build visualizations to analyze data using qualitative and quantitative techniques. The data exploration can be done interactively in 3D or programmatically using ParaView's batch processing capabilities.

ParaView was developed to analyze extremely large datasets using distributed memory computing resources. It can be run on supercomputers to analyze datasets of terascale as well as on laptops for smaller data.

ParaView is an application framework as well as a turn-key application. The ParaView code base is designed in such a way that all of its components can be reused to quickly develop vertical applications. This flexibility allows ParaView developers to quickly develop applications that have specific functionality for a specific problem domain [50].

The goals of the ParaView team include the following:

- Develop an open-source, multi-platform visualization application.
- Support distributed computation models to process large data sets.
- Create an open, flexible, and intuitive user interface.
- Develop an extensible architecture based on open standards.

3.6 Grace software

Grace is a free 2D graph plotting tool, for Unix-like operating systems (Windows with QtGrace). The package name stands for "GRaphing, Advanced Computation and Exploration of data." Grace uses the X Window System and Motif for its GUI. It has been ported to VMS, OS/2, and Windows 9*/NT/2000/XP (on Cygwin). In 1996, Linux Journal described Xmgr (an early name for Grace) as one of the two most prominent graphing packages for Linux [51].

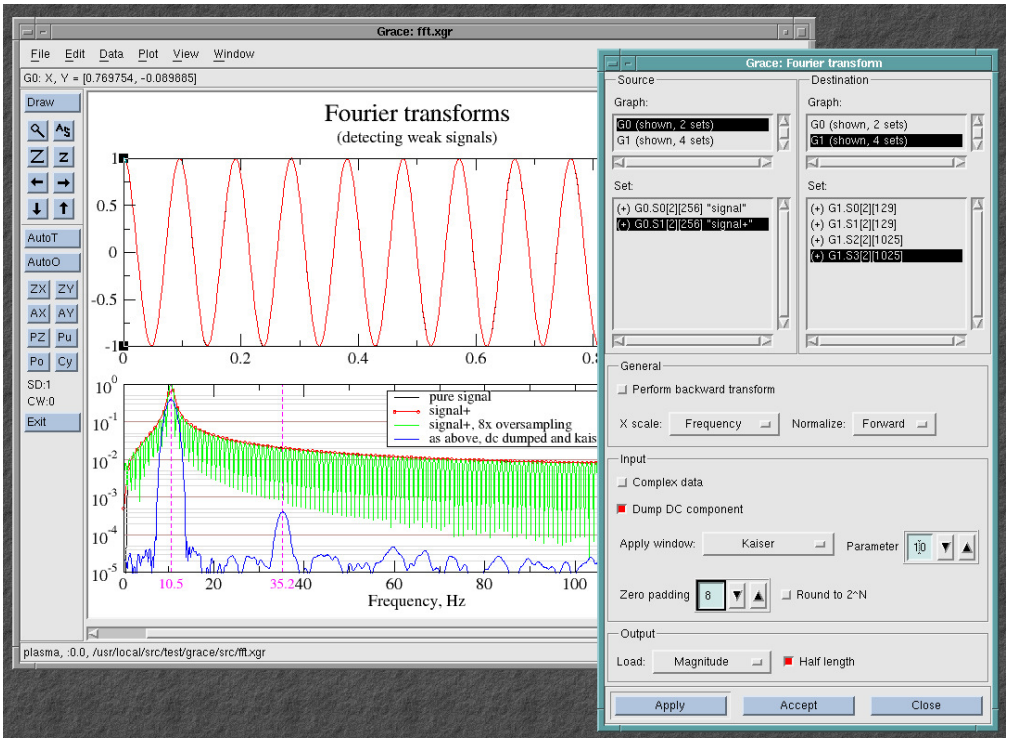

Fig.3.5- Preview of Grace, showing the Fourier transforms dialogue [52].

Conclusion

In this chapter we give a presentation of the digital tools used during this study, and all the free software used on the CFD, and we give a presentation on the boundary conditions, and the steps to follow to carry out a simulation under the Code_Saturne solver.

CHAPTER 4:
STUDY CASES

Introduction

In this chapter we used Code_Saturne calculations software for our simulation, which is a study on mesh sensitivity, and the effect of turbulence model on the numerical calculation.

We start with the introduction of the geometric shapes used (cylinder, backward-facing step). And the type of mesh that we will use (structured/ unstructured) mesh, and we use two models of turbulence $(k-\varepsilon,\ k-\omega-sst)$.

5.1 Presentation of the first case (Flow around one cylinder)

The study of the flow around a single cylinder is fundamental, one of the most studied problems in fluid mechanics or aerodynamics. And in several application of interest such as pipelines marine structures and heat exchangers, in our case we will use it to study mesh sensitivity on CFD. Therefore we will apply two different types of mesh (structured/ unstructured), see figures (5.1 and 5.2) below.

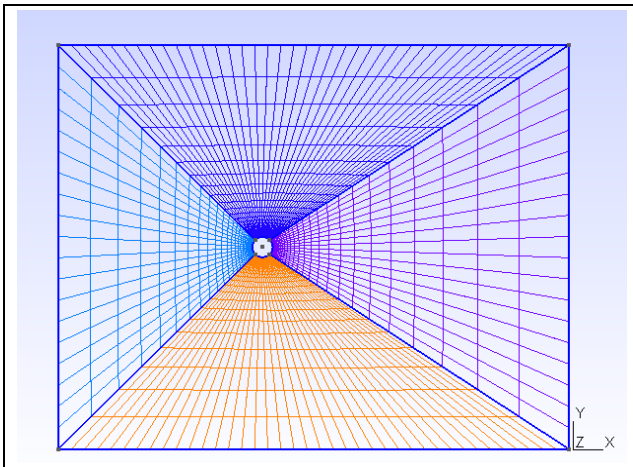

Fig.4.1 -Structured mesh in the XY plane of cylinder with Gmsh

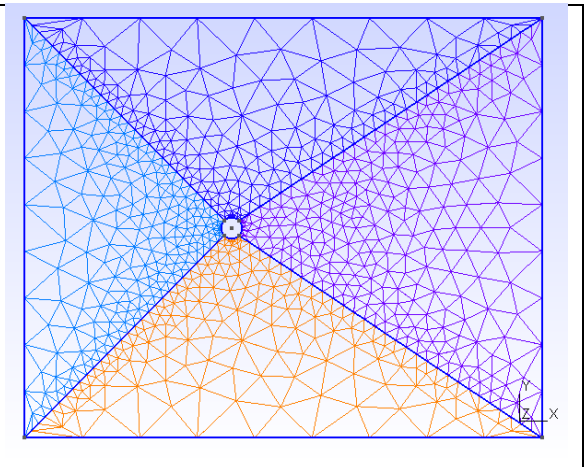

Fig.4.2 - Unstructured mesh in the XY of a cylinder with Gmsh

Then we fine-tune a grid to (coarse mesh, medium mesh, fine mesh and very fine) in the figures (4.3 to 4.9) below and we use different turbulence models.

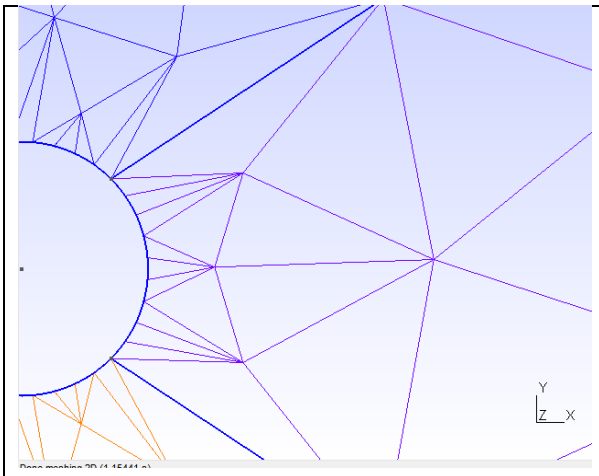

Fig.4.3-Zoom of the coarse unstructured mesh

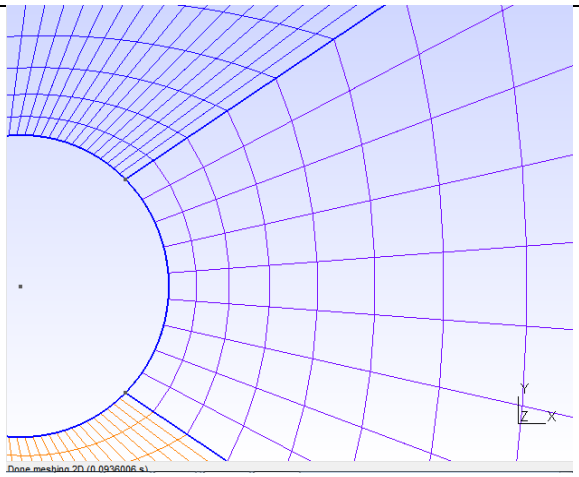

Fig.4.4 -Zoom of the coarse structured mesh

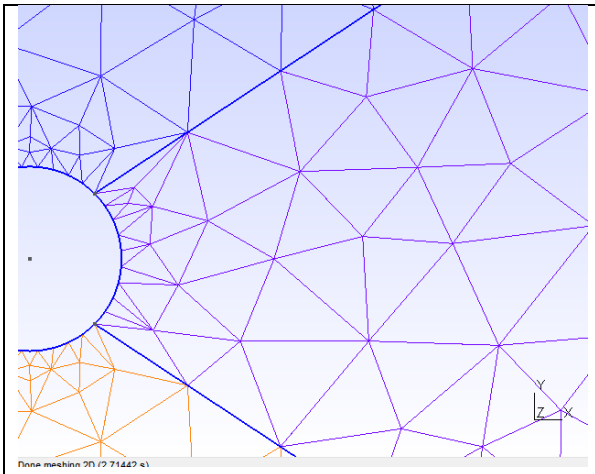

Fig.4.5 - Zoom of the medium unstructured mesh

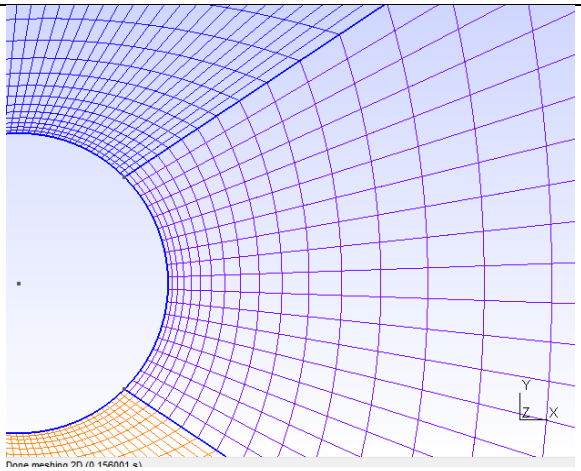

Fig.4.6- Zoom of the medium structured mesh

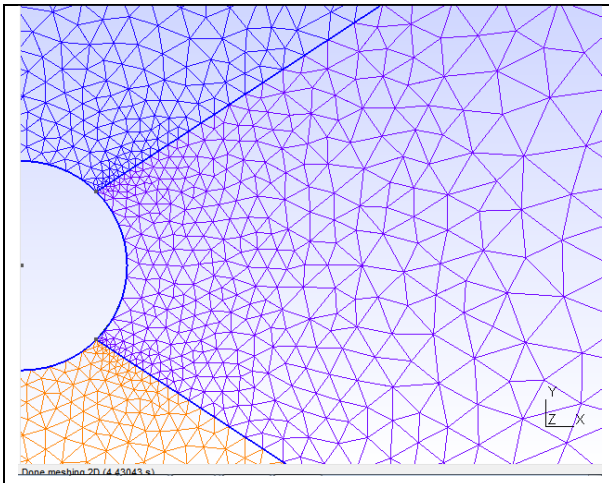

Fig.4.7-Zoom of the fine unstructured mesh

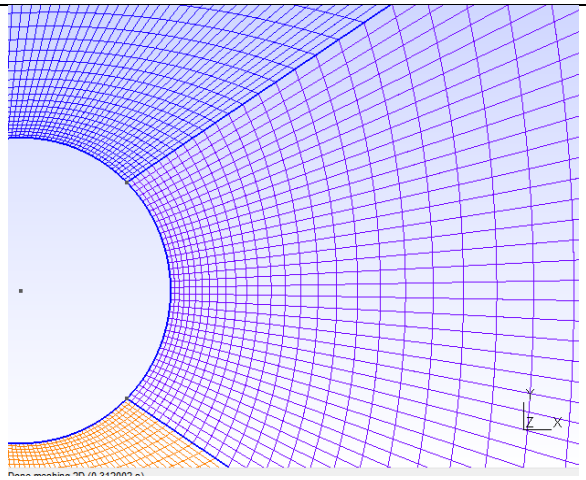

Fig.4.8-Zoom of the fine structured mesh

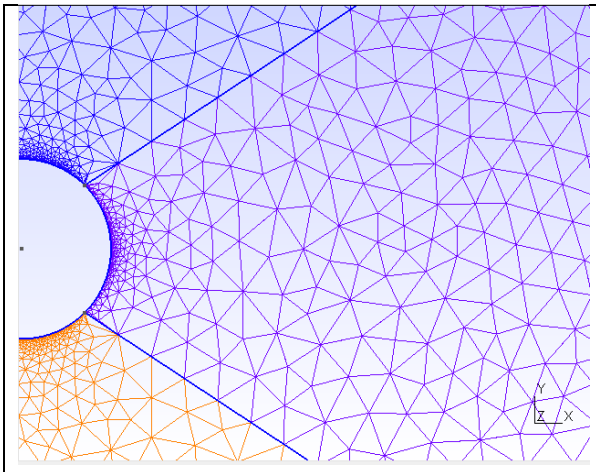

Fig.4.9-Zoom of the very fine unstructured mesh

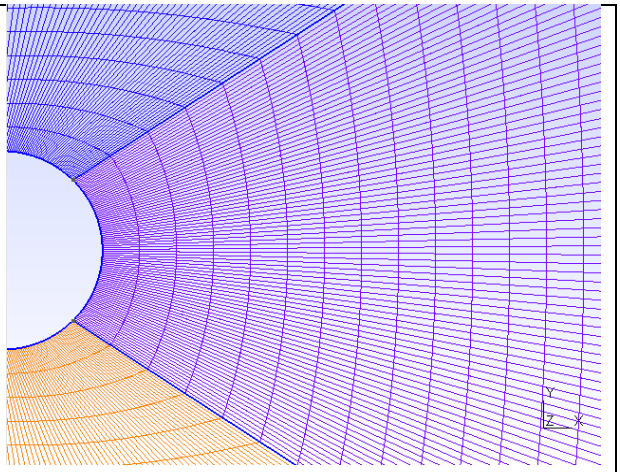

Fig.4.10 -Zoom of the very fine structured mesh

4.1.1 Physical parameters

The Reynolds number is based on the flow speed of the inlet (uniform speed without artificial and imposed turbulence) and the diameter of the cylinder we take:

$$D = 1 \ \ and \ Re = 3900.$$

4.1.2 Geometry

The computational domain used for the simulation is shown in the following figure (5.11), the dimensions of the computational domain are $(10 + 15)\, D * (10 + 10)\, D$ and the diameter of the cylinder is $1D$.

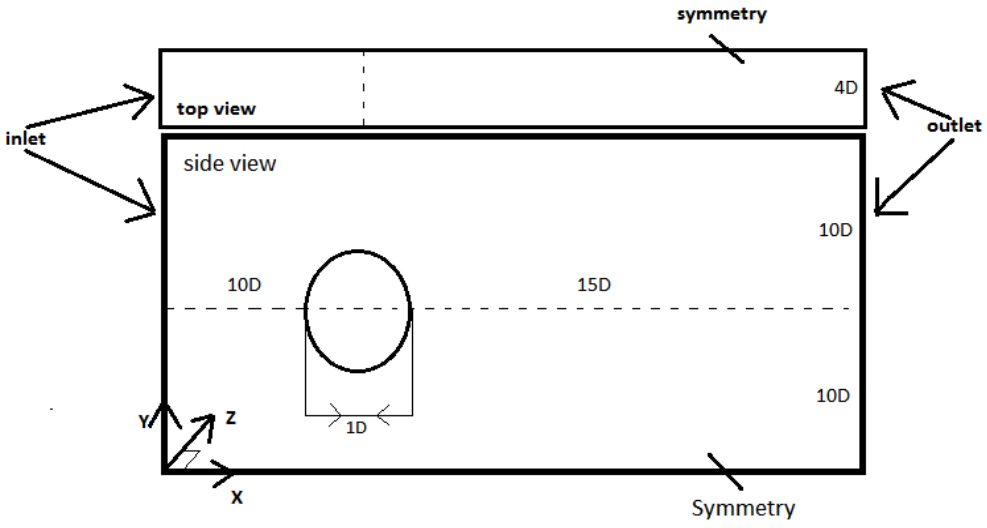

Fig.4.11 Computation domain

4.2 Presentation of the second case (Backward-facing step)

Flow over a backward-facing step (BFS) is a common phenomenon in practical engineering, such as the internal flows in diffusers, turbines, combustors, or pipes, and external flows over aircrafts, around buildings, or over stepped channels. These flows are characterized by flow separation and reattachment induced by sharp expansion of the configuration [53].

We will use it in our experiment to study mesh sensitivity, for this we used two types of mesh (structured/unstructured) shown in the figure (4.12 and 4.13) below.

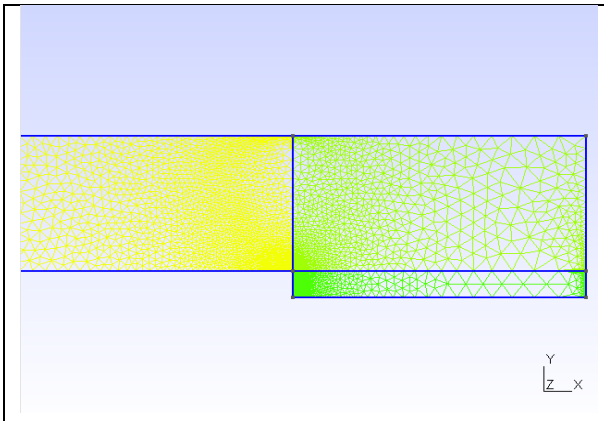

Fig.4.12-Unstructured mesh in the XY plane of a Backward-facing step with Gmsh

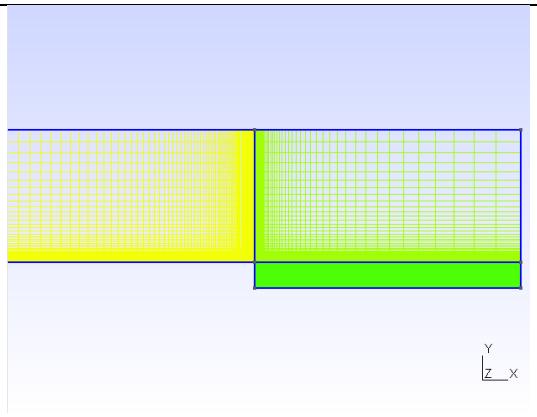

Fig.4.13-Structured mesh in the XY plane of a Backward-facing step with Gmsh

Then we fine-tune a grid to (coarse mesh, medium mesh size, and fine mesh) and we use different turbulence models.

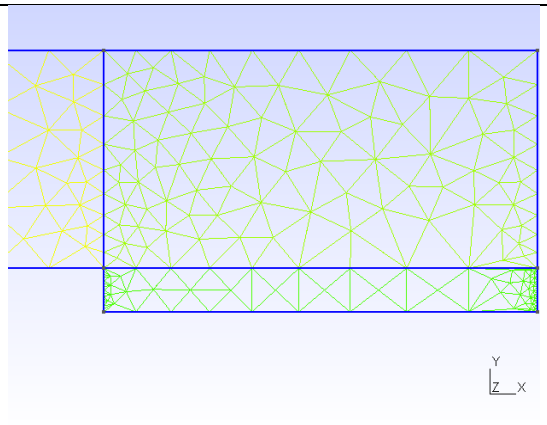

Fig.4.14-Zoom of the coarse unstructured mesh

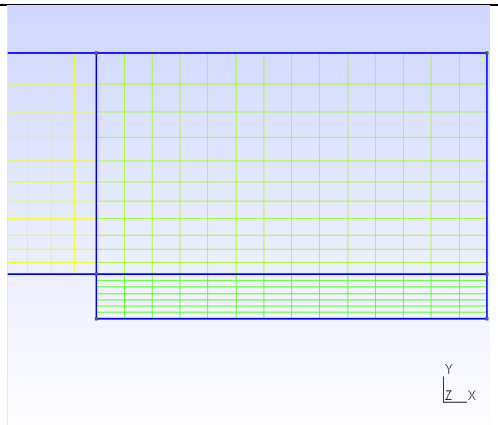

Fig.4.15-Zoom of the coarse structured mesh

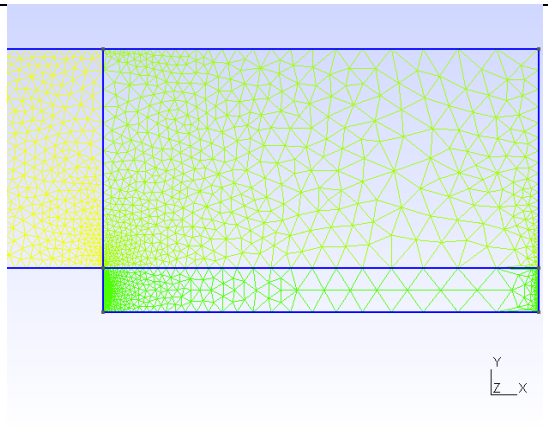

Fig.4.16- zoom of the medium unstructured mesh

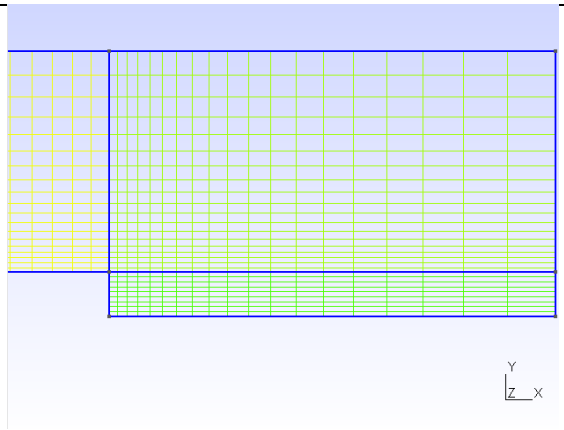

Fig.4.17- zoom of the medium structured mesh

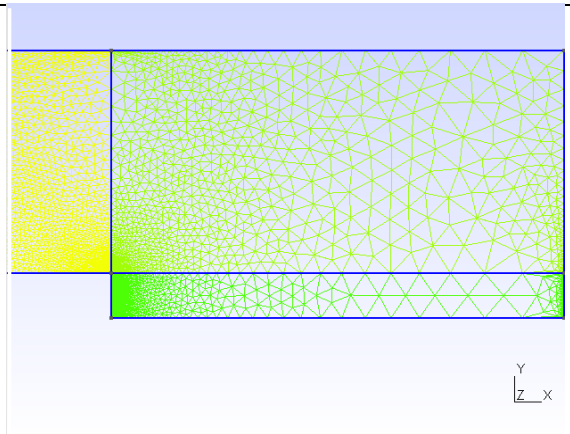

Fig.4.18- zoom of the fine unstructured mesh

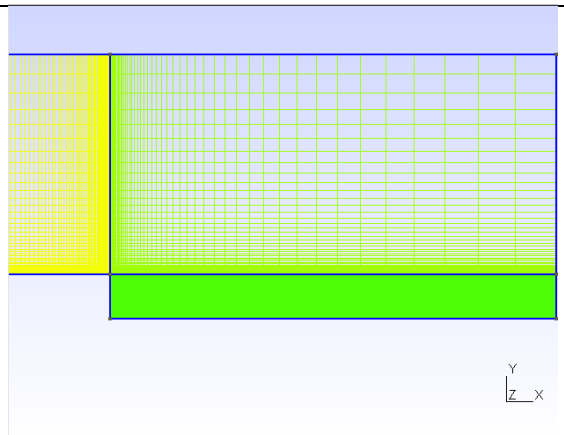

Fig.4.19- zoom of the fine structured mesh

4.2.1 Physical parameters

We will use a flow with Reynolds number $R_e = 5100$ and we will use $(k-\varepsilon,\ k-\omega-sst)$ turbulence model.

4.2.2 Geometry

The schematic view of the BFS flow in this study is shown in Figure5.20. The computational domain consisted of a total longitudinal length of $35h$ $(L_D = 25h, L_u = 10)$. L_D *and* L_u were respectively the tunnel lengths upstream and downstream of the step.

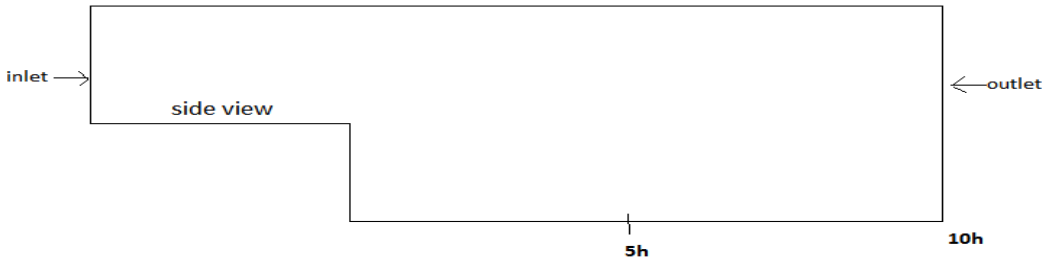

Fig.4.20-Computation domain

Conclusion

In our study, we will compute two cases to test the sensitivity of the meshes, we therefore give a description of the cases and the details of the calculation and show all the types of meshes used in our simulation.

CHAPTER 5: RESULTS AND DISCUSSION

Introduction

This chapter is dedicated to discussion and interpretation of the results of the numerical simulations carried out. We will start with the presentation of the results concerning a first case, which flows around a single cylinder with a circular cross-section and the second case which is the backward-facing step. To study the sensitivity of the mesh, we used two turbulence models ($k-\varepsilon$, $k-w-sst$) and then we will discuss the numerical results with the experimental results.

5.1 Study of the mesh sensitivity and the influence of turbulence models

One of the big problem in numerical calculation is the choice of the fineness of the mesh and of the turbulence modeling, for which the results have a good precision and to capture all the phenomena without leading to too long calculation times the mesh refinement effect is a necessary phase in determining the optimum mesh size, and the choice of turbulence model to obtain better results.

Many times we need fine mesh size near the walls and even in recirculation areas, the choice of turbulence model and mesh refinement plays an important role in the accuracy of the result and the computation time.

5.1.1The first case: flows around a cylinder

5.1.1.1Grids statistics

	Very Fine mesh (TREFIN)			Fine mesh (FIN)			Medium mesh (MOY)			Coarse mesh (GRO)		
Structured Mesh (STR)	N_{grid}	N_x	N_y	N_{grid}	N_x	N_y	N_{grid}	N_x	N_y	N_{grid}	N_x	N_y
	23384	80	80	10584	60	60	5304	40	40	2784	30	30
Unstructured Mesh (NSTR)	N_{grid}	N_x	N_y	N_{grid}	N_x	N_y	N_{grid}	N_x	N_y	N_{grid}	N_x	N_y
	27578	80	80	13454	60	60	7210	40	40	3986	30	30

Table.5.1-Statistics of the grids used for the simulations

The table 5.1 gives us all the statistics about the grids, such as number of cells, used in the simulations and from this table we see that we used the same cell number in the same direction between the structured and unstructured mesh. This is to ensure a fair comparison and to choose the best mesh type.

5.1.1.2 Computation time

	Structured Mesh (STR)				Unstructured Mesh (NSTR)			
	Very Fine mesh (TREFIN)	Fine mesh (FIN)	Medium mesh (MOY)	Coarse mesh (GRO)	Very Fine mesh (TREFIN)	Fine mesh (FIN)	Medium mesh (MOY)	Coarse mesh (GRO)
Time of calculation(S) K-ε	2042	1203	431	277	N	2080	770	391
Time of calculation (S) K-ω-SST	1935	720	431	207	N	2123	893	397

Table.5.2 –Calculation time of the first case (single cylinder)

This table shows the time it took for each type to simulate in our case. We can see (in the case of coarse meshes), that there is not much difference in computation time between the K-ε and K-ω-SST turbulence models, but the computation time increases as we increase the refinement of the mesh to reach its maximum value when we use a very fine mesh.

Note: When we used a structured very fine mesh, we get good results with K-ω-SST, with a long computation time, but when we use unstructured very fine mesh, we have a divergence in the results with different turbulence model used(K-ε, K-ω-SST) and the simulation is canceled.

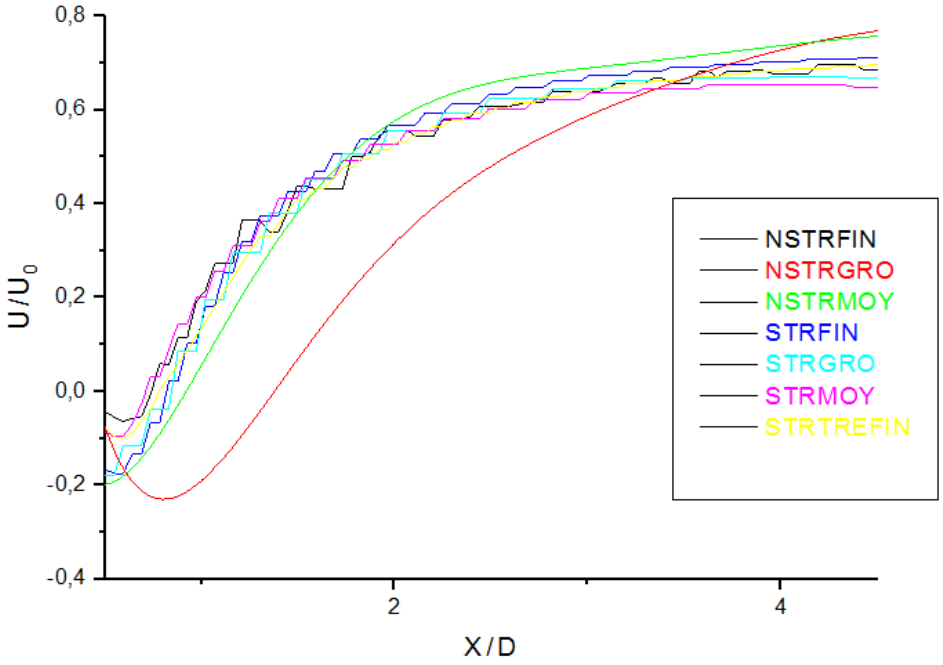

Fig.5.1- Mean stream-wise velocity along the wake centerline $(Y/D = 0)$for different meshes type, for a single cylinder at the $Re_{D,U_0} = 3900$using K-ε turbulent model

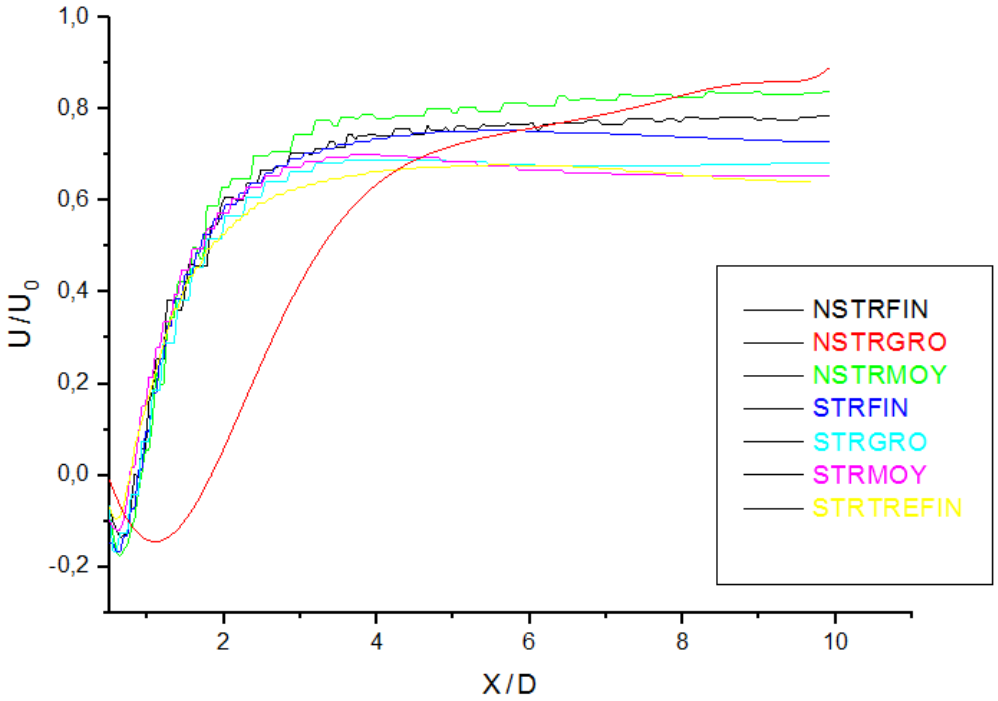

Fig.5.2- Mean stream-wise velocity along the wake centerline $(Y/D = 0)$ for different meshes type, for a single cylinder at the $Re_{D,U_0} = 3900$ using K-ω-SST turbulent model

For the sensitivity study we used two types of mesh (structured and unstructured) and four grids (coarse, medium, fine and very fine) and we used in this simulation two different turbulent models K-ε, K-ω-SST to define the best mesh and turbulent model.

The result of our numerical simulation is shown in figure 5.1and 5.2.In the first figure that we used the K-ε turbulence model, we notice that there is a big difference between the curves. The results are very far apart and we observe in the second figure that there is almost no change in the mean velocity profile, except one curve which is far from bunch and we notices the concordance between the two curves (fine and very fine mesh), figure below with k-ω-SST.

In order to gain time, we chose the fine mesh with k-ω-SST turbulence model. This combination was fast in the calculation.

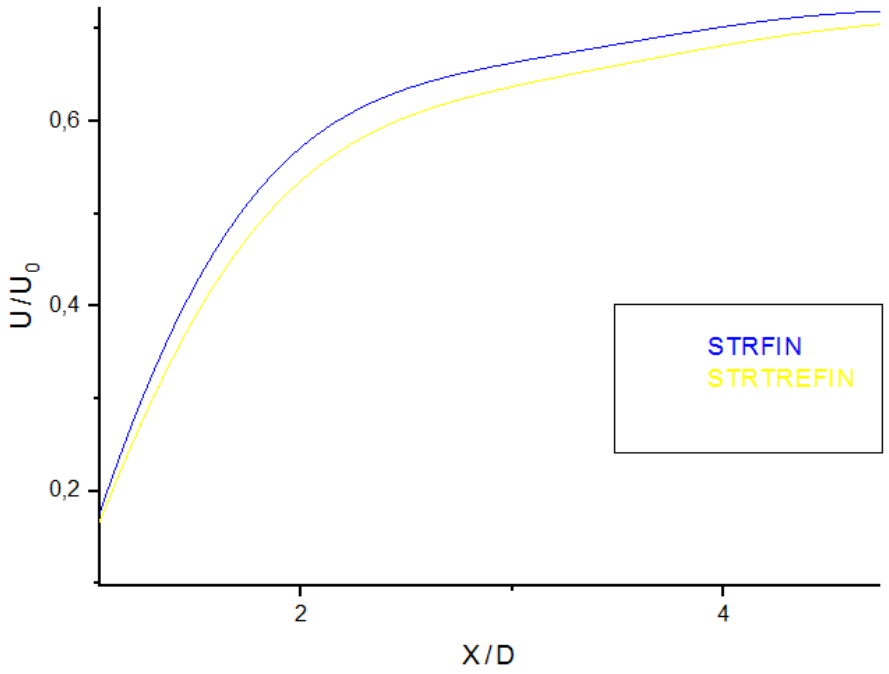

Fig.5.3-Zoom of mean stream-wise velocity along the wake centerline $(Y/D = 0)$. Blue: fine mesh, yellow :very fine mesh. With K-ω-SST turbulence model.

Study	Mode	R_e
Norberg [54]	EXP	3000
Lourenco and Shih [55]	EXP	3900
Kravchenko and Moin [56]	LES	3900
Parnaudeau et al [57]	EXP/LES	3900
Wissink and Rodi [58]	DNS	3300
Afgan et al [59]	LES	3900

Table.5.3- Previous studies used for comparison in the case of a single cylinder

5.1.1.3 Mean velocity and recirculation length

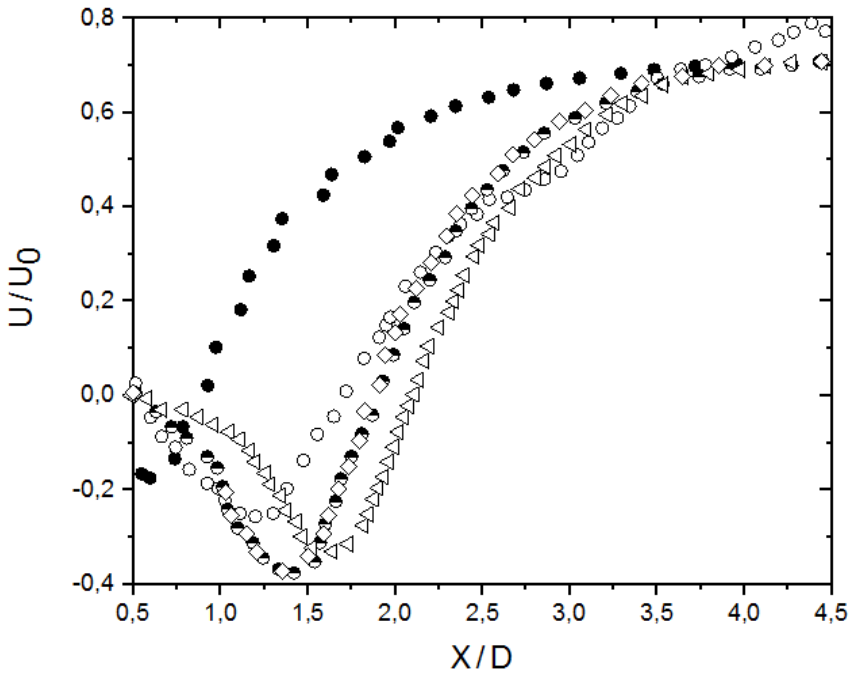

Fig.5.4-Mean stream-wise velocity along the wake centerline $(Y/D = 0)$ for a single cylinder at $R_{e_{D,u_0}} = 3900$. ●: Present study, ○: Exp Lourenco and Shih, ◓ : LES Kravchenko and Moin, △ : DNS Wissink and Rodi

To compare the results of our RANS study with the numerical and experimental studies we have plotted the average speed $\bar{u}$ in the wake axis fig below we observed that the velocity is zero at the wall and reaches the minimum negative value u_{min} in the recirculation zone, we see from the figure5.4 that the LES Kravchenko curve has the highest minimum speed, a

difference is to be noted concerning the recirculation length and the maximum return speed which is smaller than the other values. But we have the same look of speed profiles with experimental and numerical results.

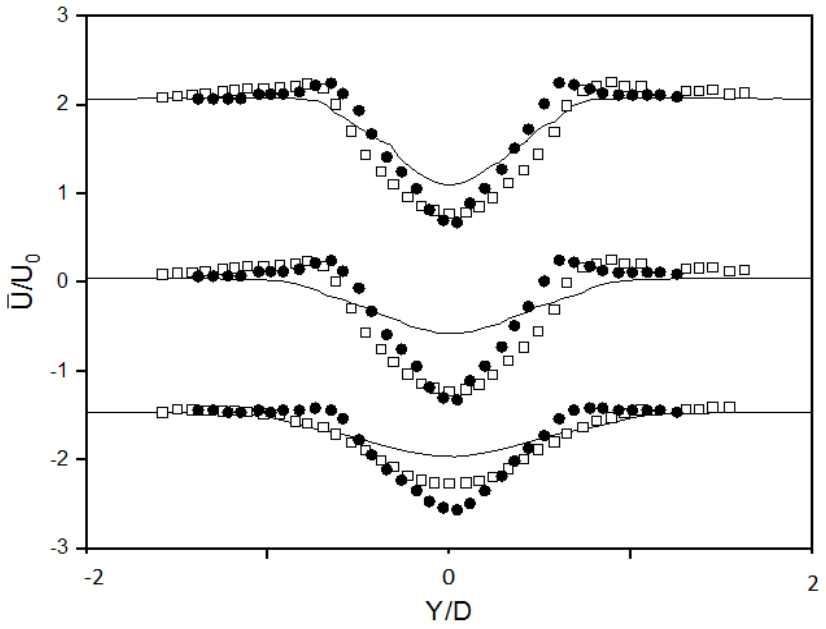

Fig.5.5- Mean stream wise velocity $(\overline{U}/U_0)$at various X/D down-stream location at $R_{D,u_0} = 3900$, −:Present study,●: EXP Lourenco and Shih, □: EXP Parnaudeau et al.

In the figures5.5 and 5.6we present the mean stream-wise $(\overline{U}/U_0)$ and crosse-stream $(\overline{V}/U_0)$ velocity profiles respectively, in the wake of the single cylinder at$R_e = 3900$, the results were taken at three points $(X/D = 1{,}06, X/D = 1{,}54, X/D = 2{,}02)$ behind the cylinder.

A "V" shaped profile is observed close to the cylinder at $(X/D = 1{,}06)$,because of the short recirculation length, this is in line with Lourenco and Shih experiment, unlike the experimental result of Parnaudeau et al which have a "U" shape profile at$(X/D = 1{,}06)$and when we move downstream, the profile changes to the "V" shape at $(X/D = 1{,}54$ and 2,02).On the other hand, comparisons between our RANS study with the K-W-SST turbulence model and the type of fine structure meshing with the experimental data for the mean crosse-stream $(\overline{V}/U_0)$velocity is shown in the figure5.6.We observe in this figure that the velocity at $(X/D = 1{,}06)$, and this phenomenon is derived away from the line of symmetry is reversed by approaching the line of symmetry at points $(X/D = 1{,}54$ and 2, 02), and our results are in accordance with the experimental result of Lourenco and Shih at $(X/D = 1{,}06)$ and with the experimental result of Parnaudeau el al. at $(X/D = 1{,}54)$and the profile at the position$(X/D = 2{,}02)$ deviates from other data always because of the short recirculation length of our results.

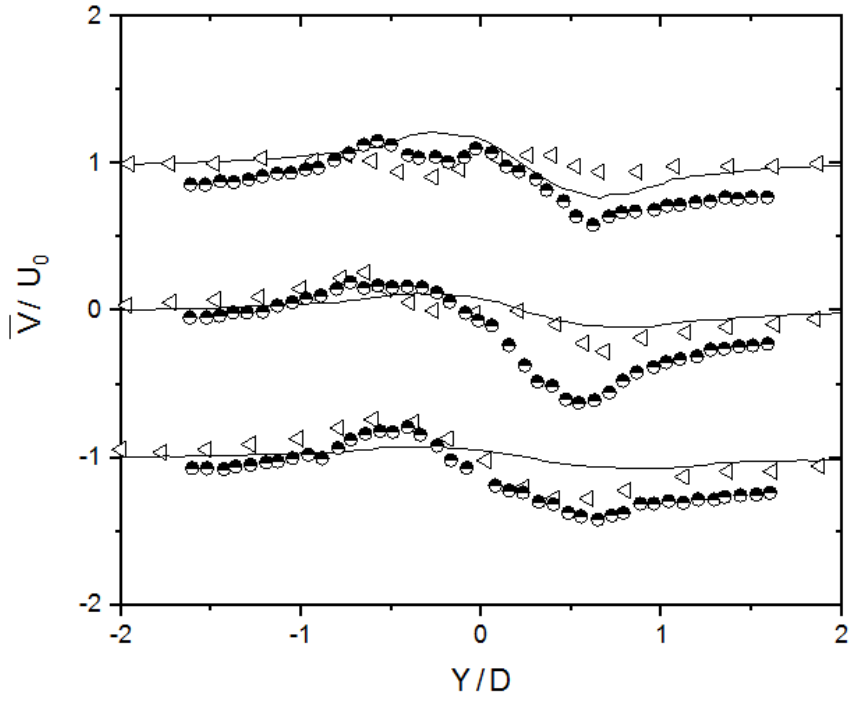

Fig.5.6-Mean cross-stream velocity ($\bar{V}/U_0$) at various X/D down-stream locations at$R_{D,u_0} = 3900$. – :Present study. ◓: EXP Lourenco and Shih, ◠: EXP Parnaudeau et al.

5.1.1.4Mean pressure coefficient

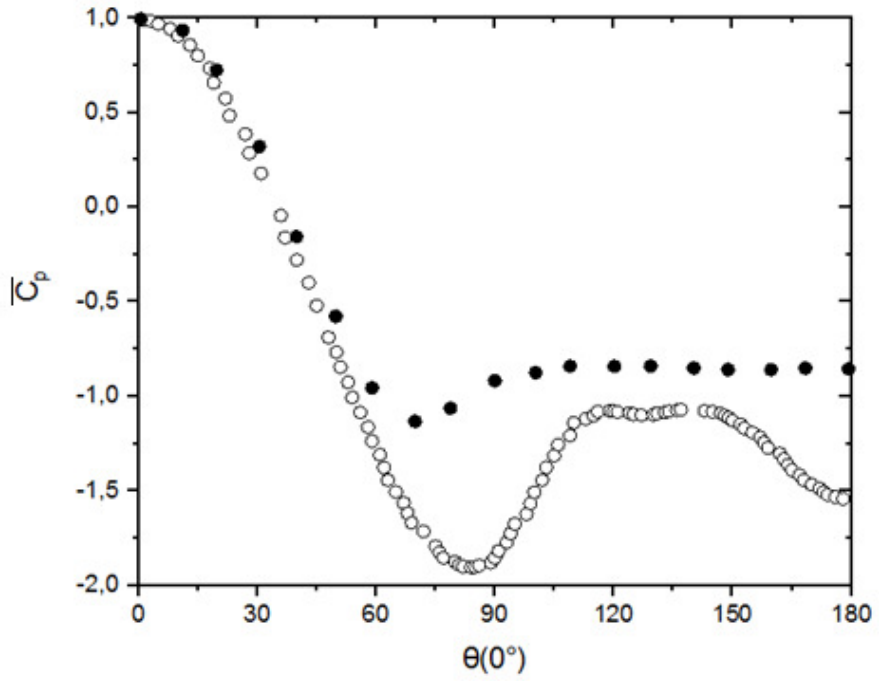

Fig.5.7- Mean pressure coefficient profile around a single cylinder.

○: Present study ($Re_{D,u_0} = 3900$) , ●: EXP Nerberg ($Re_{D,u_0} = 3000$)

The pressure distribution around the cylinder is shown in the figure 5.7 and the mathematical relation to calculate the average pressure coefficient is:

$$\overline{Cp} = 2(\bar{P} - P_{\infty})/(\rho_{\infty} u_{\infty}^2)$$

And we compared our results with Norberg experimental results at $R_{D,u_0} = 3000$.

The figure shows the distribution of the mean $\overline{Cp}$ around the cylinder surface, $\overline{Cp}$ reaches its maximum value at the leading edge $\overline{Cp}\ max$=1 for an angle $\theta = 0°$, after this angle the $\overline{Cp}$ profile decreases to a minimum value $\overline{Cp} = -1{,}87$ for an angle $\theta = 82°$, in the wake there are disparities between the numerical and experimental results because we see a depression, this discrepancy may be due to our simulation method to calculate the $\overline{Cp}$.

Note: the distribution of the $\overline{Cp}$ is symmetrical with respect to the 180° angle

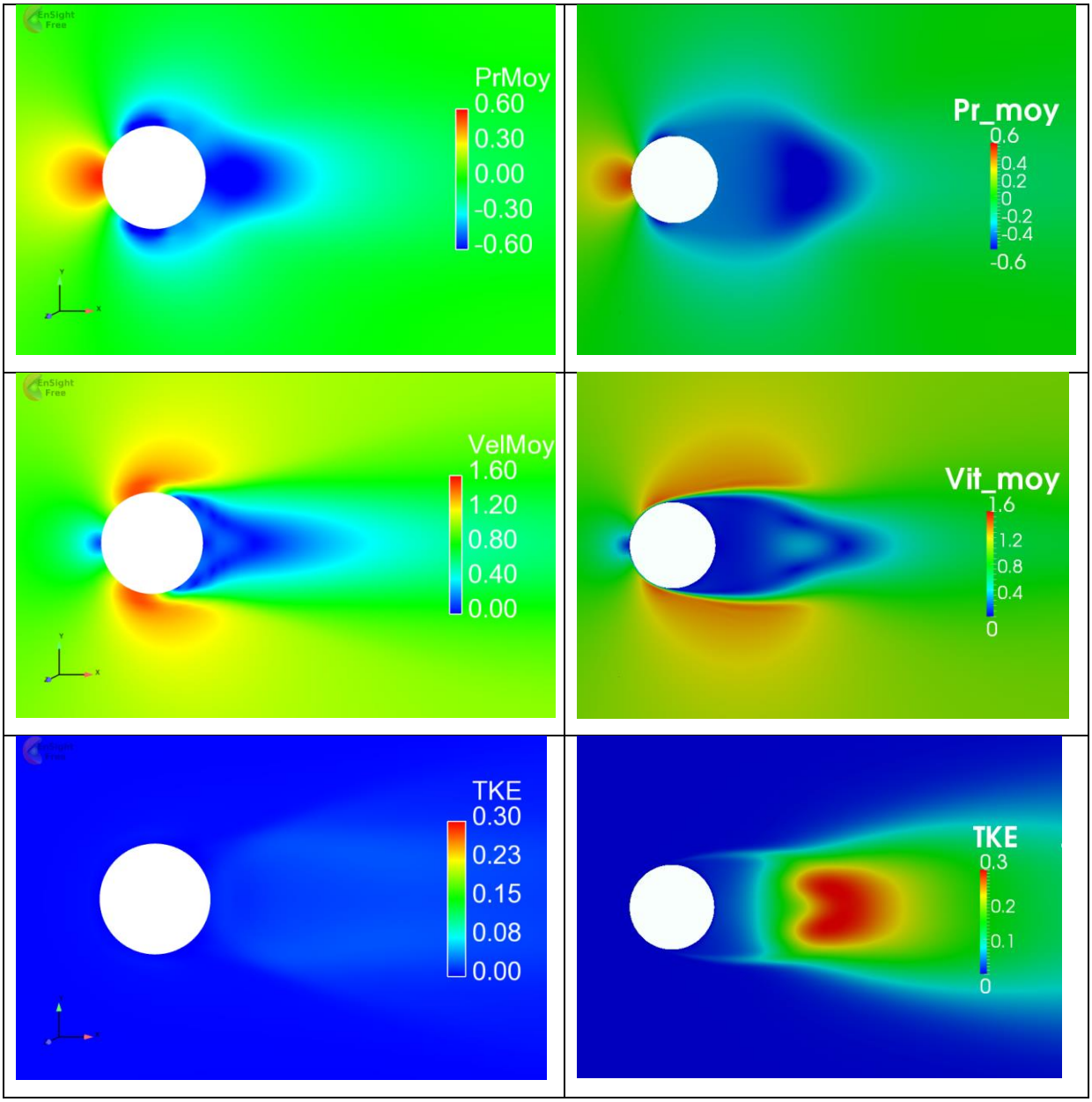

Fig.5.8- Comparison of the different flow fields. Left: Present study, right: L.E.S Afgan et al.

In figure 5.8, the flow fields (mean pressure, mean velocity and turbulent kenetic energy) of the present study were compared to the numerical results of Afgan et al.

5.1.2 The second case: Backward-facing step

5.1.2.1Grids statistics

	Fine mesh			Medium mesh			Coarse mesh		
Structured Mesh	N_{grid}	N_x	N_y	N_{grid}	N_x	N_y	N_{grid}	N_x	N_y
	5048	50	65	3181	40	47	2178	35	45
Unstructured Mesh	N_{grid}	N_x	N_y	N_{grid}	N_x	N_y	N_{grid}	N_x	N_y
	7238	50	65	4650	40	47	3666	35	45

Table.5.4-Statistics of the grids used for the simulations

For the second case Backward-facing step we use the same line number between the structured and unstructured mesh to compared and confirmed the result of the first simulation to choose the best mesh type and turbulence model.

5.1.2.2 Computation time

	Structured Mesh			Unstructured Mesh		
	Fine mesh	Medium mesh	Coarse mesh	Fine mesh	Medium mesh	Coarse mesh
Time of calculation(S) K-ε	293	192	128	2233	1475	1097
Time of calculation (S) K-ω-SST	294	185	128	2487	1394	1264

Table.5.5 –Calculation time of the second case (Backward-facing step)

This table shows the time it took for each type to simulate the second case (Backward-facing step). We can see that there is not much difference in computation time between the K-ε and

K-ω-SST turbulence models, but the difference is clear between structured and unstructured meshes and the computation time increases as we increase the refinement of the mesh.

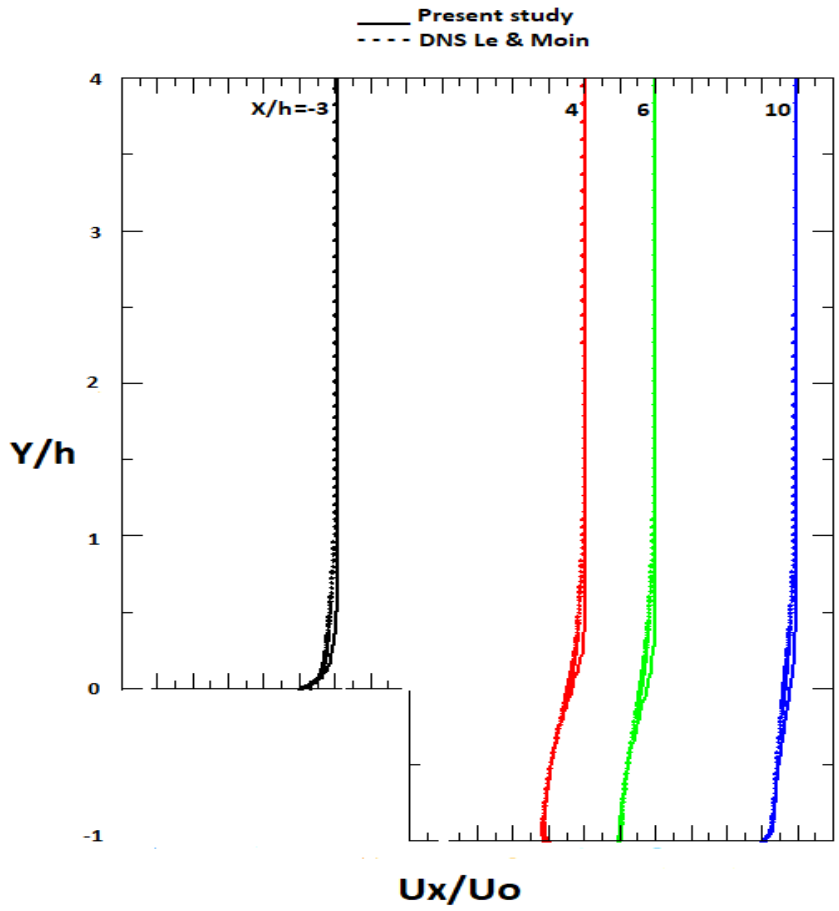

Fig.5.9-Comparison of mean stream wise velocity profile

In the figure 5.9 we present a comparison between our RANS study with the DNS of Le and Moin [60] for the mean stream wise velocity profiles. The comparison is made at four representation location in the recirculation reattachment and recovery region we have the same look of speed profiles with experimental result. A good agreement between our results and the experimental results is obtained at all location.

GENERAL CONCLUSION

General conclusion

In This work we studied with a numerical simulation provided by the free software Code_Saturne, the mesh sensitivity. The objective of this work is to choose the best mesh type and turbulence modeling to use in (CFD). For this study we carried out the simulations in two different forms, the first case is the flow around a single cylinder and the second case is the Backward-facing step. We used two different turbulence model ($k-\varepsilon, k-\omega SST$) and different mesh type (structured and unstructured).We used the same line cells number between the structured and unstructured mesh, this is to ensure a fair comparison and to choose the best mesh type. At the end of the simulation, we noted the time it took to calculate each type, although the difference in the time of compute was not big but the results of longitudinal mean velocity and the results showed a great convergence between the structured fine and very fine mesh. In order to gain time, we chose the structured fine mesh and the k-ω-SST turbulence model because it was fast in the calculation.

The first case concerns a simulation of a flow around a single cylinder. We showed a comparison of our simulation with the experimental results. We noticed the effect of the type mesh and the turbulent model over the finale results.

The flow is modeled by the differential equations with partial derivatives of mass conservation and movement quantities, for the discretization of the equation Code_Saturne used the finite volumes method. After showing the simulation results we have plotted the velocity and pressure curves, as well as the longitudinal and transverse velocity fields, the recirculation length and the mean pressure distribution around the cylinder surface.

Finally, the results obtained are in good agreement with the experimental and numerical results. In addition, some very interesting phenomena have been observed that the type of fine-structured mesh and the $k-\omega-SST$ provides good results to help understand flow behavior and to explain physical phenomena for the future work. Concerning the mesh sensitivity and the choice of the turbulence models, this is in order to obtain the best results.

Bibliography

[1] Wangda Zuo. Introduction of Computational Fluid Dynamics. Research paper, FAU Erlangen-Nürnberg, JASS 05, St. Petersburg. Ru.

[2] Essam E. Khalil. (2012). CFD History and Applications. CFD Letters, Vol. 4(2) 2012.

[3] Sallam, Ahmed M., Hwang, Ned H.C. (1984). Human red blood cell hemolysis in a turbulent shear flow: Contribution of Reynolds shear stresses. Biorheology, vol. 21, no. 6, pp. 783-797, 1984.

[4] Yi He, Andrew E. Bayly, Ali Hassanpour, Michael Fairweather, Frans Muller. (2020). Flow behavior of an agitated tubular reactor using a novel dynamic mesh based CFD model. Chemical Engineering Science, Volume 212, 2 February 2020, 115333.

[5] Hao Li, Li Rong, Guoqiang Zhang. (2019). CFD prediction of convective heat transfer and pressure drop of pigs in group using virtual wind tunnels: Influence of grid resolution and turbulence modeling. Biosystems engineering 184 (2019) 69-80.

[6] Jun Zhang, Farzin Darihaki, Siamack A. Shirazi. (2019). A comprehensive CFD-based erosion prediction for sharp bend geometry with examination of grid effect. Wear 430–431 (2019) 191–201.

[7] Panagiotis Tsoutsanis, Ioannis W. Kokkinakis, László Könözsy, Dimitris Drikakis, Robin J. R. Williams, David L. Youngs. (2015). Comparison of structured- and unstructured-grid, compressible and incompressible methods using the vortex pairing problem. Computer Methods in Applied Mechanics and Engineering. Volume 293, 15 August 2015, Pages 207-231.

[8] IvanaMartić, NastiaDegiuli, Andrea Farkas, JosipBašić. (2017). Mesh Sensitivity Analysis for the Numerical Simulation of a Damaged Ship Model. Proceedings of the Twenty-seventh (2017) International Ocean and Polar Engineering Conference San Francisco, CA, USA, June 25-30, 2017.

[9] Mulualem G. Gebreslassie, Gavin R. Tabor, Michael R. Belmont. (2012). CFD Simulations for Sensitivity Analysis of Different Parameters to the Wake Characteristics of Tidal Turbine. Open Journal of Fluid Dynamics, 2012, 2, 56-64.

[10] Rui Zhang, Yongjie Zhang, KheePoh Lam, David H. Archer. (2010). A prototype mesh generation tool for CFD simulations in architecture domain. Building and Environment, Volume 45, Issue 10, October 2010, Pages 2253-2262.

[11] Jia-Wei Han, Wen-Ying Zhu, Zeng-Tao Ji. (2019). Comparison of veracity and application of different CFD turbulence models for refrigerated transport. Artificial

Intelligence in Agriculture, Volume 3, September 2019, Pages 11-17.

[12] Olubunmi Popoola, Yiding Cao. (2016). The influence of turbulence models on the accuracy of CFD analysis of a reciprocating mechanism driven heat loop. Case Studies in Thermal Engineering, Volume 8, September 2016, Pages 277-290.

[13] Attila Kiss, Attila Aszódi. (2012). Sensitivity studies on CFD analysis for heat transfer of supercritical water flowing in vertical tubes. OECD Nuclear Energy Agency & IAEA Joint Workshop: CFD4NRS-4Daejeon, Korea**,** 10–12 September 2012.

[14] T. Bartzanas, C. Kittas, A. A. Sapounas, Ch. Nikita-Martzopoulou. (2007). Analysis of airflow through experimental rural buildings: Sensitivity to turbulence models. Biosystems Engineering, Volume 97, Issue 2, June 2007, Pages 229-239.

[15] Mario Knoll, Hannes Gerhardter, Christoph Hochenauer, Peter Tomazic. (2020). Influences of turbulence modeling on particle-wall contacts in numerical simulations of industrial furnaces for thermal particle treatment. Powder Technology, Volume 373, August 2020, Pages 497-509.

[16] Håkan Gustavsson. (2016). Introduction to Turbulence. Report, Division of Fluid Mechanics, Luleå University of Technology.

[17] www.aviationknowledge.wikidot.com

[18] https://www.nuclear-power.net/nuclear-engineering/fluid-dynamics/turbulent-flow/characteristics-of-turbulent-flow/: 04/10/2020

[19] https://whatis.techtarget.com/definition/computational-fluid-dynamics-CFD

[20] www.fetchcfd.com

[21] https://www.manchestercfd.co.uk/post/all-there-is-to-know-about-different-mesh-types-in-cfd: 27/08/2020

[22] www.afs.enea.it

[23] https://www.gidhome.com/

[24] www.sciencedirect.com/structured-mesh

[25] Mavriplis, D.J. (1996). Mesh Generation and adaptivity for complex geometries and flows. Handbook of Computational Fluid Mechanics. 1996, Pages 417-459.

[26] www.researchgate.net

[27] www.gmsh.info

[28] Bern Marshall, Plassmann Paul. (2000). Mesh Generation. Handbook of Computational Geometry. 2000, Pages 291-332.

[29] Orszag, Steven A. (1970). Analytical Theories of Turbulence. Journal of Fluid Mechanics. 41(2) 1970, 363–386.

[30] Moin, P., Mahesh, K., 1998. Direct numerical solution: a tool in turbulence research.

Annual Review of Fluid Mechanics, 30, 1998, pp 539-578.

[31] Li, C. et al., (2013) Renewable Energy 51,317-330

[32] https://www.sciencedirect.com/topics/engineering/reynolds-averaged-navier-stokes

[33] Tennekes, H., Lumley, J. L. (1972). A first course in turbulence. The MIT Press. Cambridge, Mass. and London, UK.

[34] www.editions.covecollective.org

[35] Cuong Nguyen.(2005). Turbulence Modeling. Report, November 05, 2005.

[36] Kuzmin, D., Mierka, O., Turek, S., (2007). On the Implementation of Turbulence Model in k−ε Incompressible Flow Solvers Based on a Finite Element Discretization. Int. J. Computing Science and Mathematics. 2007 Vol.1 No.2/3/4.

[37] Zeghib, A., Talbi, K., (2008). Comparaison des différents modèles de turbulence d'un écoulement aérodynamique dans un cyclone, Revue des Energies Renouvelables CISM'08 Oum El Bouaghi, 2008 pp.311 – 324.

[38] Wilcox, D. C. (2008). Formulation of the k–ω Turbulence Model Revisited. AIAA Journal, Vol. 46, No. 11.

[39] http://hmf.enseeiht.fr/travaux/beiepe/book/export/html/1124. Date de la dernière consultation du site: 06/10/2020.

[40] Menter, F. R., Kuntz, M., Langtry, R., 2003. Ten Years of Industrial Experience with the SST Turbulence Model. Turbulence, Heat and Mass Transfer 4.

[41] R. Eymard, T Gallouët and R. Herbin. 2000Finite volume method. Handbook of Numerical Analysis, 7.

[42] Rahmani Zakaria, Kahil Yacine, Benlefki Abdelkrim. (2020). Étude numérique d'écoulement turbulent autour de quatre cylindres en configuration carré. Recueil de mécanique, Volume 4, Numéro 2, Pages 359-373.

[43] Geuzaine, Christophe; Remacle, Jean-François (2009). Gmsh: A 3-D finite element mesh generator with built-in pre- and post-processing facilities. International Journal for Numerical Methods in Engineering. Volume79, Issue11. 10 September 2009, Pages 1309-1331.

[44] https://www.code-saturne.org/cms/ : 24/10/2020

[45] Daniel Zwillinger (1997). Handbook of Differential Equations. Academic Press. 1997. Hardcover ISBN:9780127843964

[46] https://www.sciencedirect.com/topics/engineering/boundary-condition: 04/10/2020

[47] www.ansys.com

[48] https://www.ansys.com/-/media/ansys/corporate/resourcelibrary/brochure/brochure-ansys-ensight.pdf : 24/10/2020

[49] https://www.dkrz.de/mms/pdf/vis/paraview.pdf

[50] Utkarsh Ayachit (2015). The ParaView Guide: A Parallel Visualization Application. Kitware, 2015.

[51] https://plasma-gate.weizmann.ac.il/Grace/

[52] www.wikiwand.com/en/Grace_(plotting_tool)

[53] Fang-fang Wang, Shi-qiang Wu, Sen-lin Zhu. (1019). Numerical simulation of flow separation over a backward-facing step with high Reynolds number. Water Science and Engineering, Volume 12, Issue 2, June 2019, Pages 145-154.

[54] C. Norberg. (1994). An experimental investigation of flow around a circular cylinder: influence of aspect ratio. Journal of Fluid Mechanics, 258:287–316, 1994.

[55] L. M. Lourenco and C. Shih. (1993). Characteristics of the plane turbulent near wake of a circular cylinder, a particle image velocimetry study. Published in Beaudan and Moin, 1993.

[56] A. G. Kravchenko and P. Moin. (2000). Numerical studies of flow around a circular cylinder at Re=3900. Physics of Fluids, 12:403–417, 2000.

[57] P. Parnaudeau, J. Carlier, D. Heitz et E. Lamballais. (2008). Experimental and numerical studies of the flow over a circular cylinder at Reynolds number 3900. Physics of Fluids, 20:085101, 2008.

[58] J. G. Wissink and W. Rodi. (2008). Numerical study of the near wake of a circular cylinder. International Journal of Heat and Fluid Flow, 29:1060–1070, 2008.

[59] I. Afgan, Y. Kahil, S. Benhamadouche, P. Sagaut. (2011). Large eddy simulation of the flow around single and two side-by-side cylinders at subcritical Reynolds numbers. PHYSICS OF FLUIDS 23, 075101, 2011.

[60] Hung Le, Parviz Moin and John Kim (1997). Direct numerical simulation of turbulent flow over a backward-facing step. J. Fluid Mech. (1997), vol. 330, pp. 349-374.

Abstract

This work aims to study the mesh sensitivity and the influence of turbulence model on numerical calculation. We study the flow by the RANS approach using the Code_Saturne to solve the system of equations governing the flow. After having realized two cases, the first one is a single cylinder and the second one is a backward-facing step, we use different mesh type and different turbulence model with a Reynolds number of 3900 for a cylinder and 5100 for the backward-facing step. After comparing the results obtained from our experience with the experimental results, we concluded that the fine mesh type and $K-\omega-SST$ provide the best results and with less calculation time.

Keywords: One cylinder, turbulent flow, RANS, Code_Saturne, Backward-facing step, Reynolds number.

ملخص

يهدف هذا العمل إلى دراسة حساسية الشبكة وتأثير نموذج الاضطراب على الحساب العددي. ندرس التدفق من خلال نهج RANS باستخدام Code_Saturne لحل نظام المعادلات التي تحكم التدفق ، وبعد أن أدركنا حالتين ، الأولى عبارة عن أسطوانة واحدة والثانية هي خطوة للخلف ، نستخدم نوع شبكة مختلفة و نموذج اضطراب مختلف برقم رينولدز 3900 للاسطوانة و 5100 للخطوة المواجهة للخلف. بعد مقارنة النتائج التي تم الحصول عليها من النتائج التجريبية ، توصلنا إلى أن نوع الشبكة الدقيقة ونموذج K-ω-SST يوفران أفضل النتائج مع وقت حساب أقل.

الكلمات المفتاحية : الجريان المضطرب , رقم رينولدز , اسطوانة واحدة , ر.ا.ن.س , الشبكة الدقيقة , خطوة للخلف

Résumé

Ce travail vise à étudier la sensibilité du maillage et l'influence du modèle de turbulence sur le calcul numérique. Nous étudions l'écoulement par l'approche RANS en utilisant le code de calcul Code_Saturne pour résoudre le système d'équations régissant l'écoulement. Après avoir réalisé les deux cas : le premier est un cylindre unique et le second est une marche descendante, nous utilisons différents type de maillages et différents modèle de turbulence avec un nombre de Reynolds de 3900 pour un cylindre et 5100 pour la marche. Après avoir comparé les résultats obtenus par notre simulation avec les résultats expérimentaux, nous avons conclu que le type de maille fine et le model K-ω-SST fournissent les meilleurs résultats et avec moins de temps de calcul.

Mots clés: Cylindre isolé, écoulement turbulent, RANS, Code_Saturne, marche descendante, nombre de Reynolds.